

## ANOMALOUS HIGGS COUPLINGS

M.C. GONZALEZ-GARCIA \*

*Instituto de Física Corpuscular IFIC/CSIC,  
 Departament de Física Teòrica,  
 Universitat de València, 46100 Burjassot, València, Spain.*

Received (received date)

Revised (revised date)

We review the effects of new effective interactions on the Higgs boson phenomenology. New physics in the electroweak bosonic sector is expected to induce additional interactions between the Higgs doublet field and the electroweak gauge bosons leading to anomalous Higgs couplings as well as to anomalous gauge–boson self–interactions. Using a linearly realized  $SU(2)_L \times U(1)_Y$  invariant effective Lagrangian to describe the bosonic sector of the Standard Model, we review the effects of the new effective interactions on the Higgs boson production rates and decay modes. We summarize the results from searches for the new Higgs signatures induced by the anomalous interactions in order to constrain the scale of new physics in particular at CERN LEP and Fermilab Tevatron colliders.

### 1. Introduction

The Standard Model (SM) of the electroweak interactions based on the gauge group  $SU(2)_L \times U(1)_Y$  has proven to be astonishingly successful in describing all the available precision experimental data <sup>1</sup>. This applies particularly to the predictions of the couplings of the gauge bosons to the matter fermions. The recent measurements at LEP II and the Tevatron collider of the gauge–boson self–couplings, also shed some light on the correctness of the SM predictions for the interactions on the gauge sector of the theory.

On the other hand, despite we know that the weak gauge bosons,  $Z$  and  $W$ , are massive and, in consequence, the electroweak gauge symmetry must be broken at low scales, the precise mechanism of the electroweak symmetry breaking still remains one of the most important open questions of the theory. In the SM, the breaking is realized via the so–called Higgs mechanism in which an scalar  $SU(2)$ –doublet, the Higgs boson, is introduced *ad hoc* and the symmetry is spontaneously broken by the vacuum expectation value of the Higgs field (VEV). In this particular realization, the precise form of the Higgs couplings to the gauge bosons and the self–couplings of the scalar are completely determined in terms of one free parameter which can be chosen to be the Higgs mass  $m_H$  (or its quartic self–coupling  $\lambda$ ). However, in this simple realization, the theory presents “naturalness” problems since the running

---

\*concha.gonzalez@ific.uv.es

Higgs mass is quadratically divergent with the scale. This implies the necessity of large fine-tuning in order to keep the theory perturbative, or, conversely, the existence of a cut-off scale  $\Lambda$  above which new physics must appear.

Although we do not know the specific form of this theory which will supersede the SM, we can always parametrize its low-energy effects by means of an effective Lagrangian<sup>2</sup>. The effective Lagrangian approach is a model-independent way to describe new physics that is expected to manifest itself directly at an energy scale  $\Lambda$ , larger than the scale at which the experiments are performed. The effective Lagrangian depends on the particle content at low energies, as well as on the symmetries of the low-energy theory. For instance, if the electroweak symmetry breaking is due to a heavy (strongly interacting) Higgs boson, which can be effectively removed from the physical low-energy spectrum, or to no fundamental Higgs scalar at all, one is led to consider the most general effective Lagrangian which employs a nonlinear representation of the spontaneously broken  $SU(2)_L \otimes U(1)_Y$  gauge symmetry<sup>3</sup>. In this case the resulting chiral Lagrangian is a non-renormalizable non-linear  $\sigma$  model coupled in a gauge-invariant way to the Yang-Mills theory. If, on the other hand, there is a light scalar Higgs doublet in the spectrum, the  $SU(2)_L \otimes U(1)_Y$  symmetry must be realized linearly in the effective theory<sup>4</sup>.

In constructing the Lagrangian we will maintain most of the features of the SM. We will assume that the  $\gamma$ ,  $W$  and  $Z$  are the gauge bosons of a  $SU(2)_L \times U(1)_Y$  local symmetry which is broken spontaneously because some order parameter, transforming as a doublet under  $SU(2)_L$ , acquires a VEV. In other words, we will consider the possibility of having a light Higgs boson. Hence, we will use a linear<sup>4,5</sup> realization of the  $SU(2)_L \times U(1)_Y$  gauge symmetry which for the symmetry breaking sector we parametrized by a SM-like Higgs doublet field. In the usual effective Lagrangian language, at low energy we describe the effects of the new physics, which will manifest itself directly only at scales above  $\Lambda$ , by including in the Lagrangian higher-dimension operators. In constructing these operators we will use as building blocks the gauge-boson and the Higgs fields while keeping the fermionic sector unchanged. The lowest order operators which can be built without fermions are of dimension six.

In this review we will concentrate on the effects of the new effective interactions on the Higgs boson phenomenology and “vice-versa” how the results from searches of the characteristic new signatures for the Higgs boson induced by the new interactions, can be used to constrain the scale of new physics. Anomalous Higgs boson couplings have been studied in Higgs and  $Z^0$  boson decays<sup>6</sup>, and in  $e^+e^-$ <sup>7,8,9,10,11</sup>,  $p\bar{p}$ <sup>12,13,14</sup> and  $\gamma\gamma$  colliders<sup>15</sup>.

The outline of the paper is as follows. In Sec. 2 we describe the effective Lagrangian which we will be using and which contains eleven dimension-six operators with unknown coefficients. Four of these operators,  $\mathcal{O}_{\Phi,1}$ ,  $\mathcal{O}_{DW}$ ,  $\mathcal{O}_{DB}$ , and  $\mathcal{O}_{BW}$ , modify the gauge-boson two-point functions at tree level while three operators,  $\mathcal{O}_{WWW}$ ,  $\mathcal{O}_W$ , and  $\mathcal{O}_B$ , enter at lower order in the gauge-boson three-point functions. These operators can be directly constrained by their tree-level contributions

to existing low-energy observables as well as to the direct gauge-boson production at the Tevatron Collider and LEP II. In Secs. 2.2 and 2.3 we summarize these constraints. Four operators,  $\mathcal{O}_{WW}$ ,  $\mathcal{O}_{BB}$ ,  $\mathcal{O}_W$ , and  $\mathcal{O}_B$ , modify the Higgs couplings to the gauge bosons and their effects can be studied by directly searching for the new Higgs signatures they induce. Section 3 presents the effects of these four operators in the expected production rates of the Higgs boson at colliders (Sec. 3.3) and in its decay modes (Sec. 3.2). Section 4 contains the results from the study of specific signatures at the Tevatron and LEP II. One of the most interesting features associated with the presence of these operators is the enhancement of the Higgs decay rate in two photons that makes the Higgs searches particularly clean at hadron colliders. The aim of this section is to illustrate how existing data on some final states containing photons such as :  $p\bar{p} \rightarrow j\bar{j}\gamma\gamma$ ,  $p\bar{p} \rightarrow \gamma\gamma + \cancel{E}_T$ ,  $p\bar{p} \rightarrow \gamma\gamma\gamma$  and  $e^+e^- \rightarrow \gamma\gamma\gamma$  at the Tevatron and LEP II can be used to place limits on the values of the coefficients of the higher-dimension operators, or, in other words, on the scale of new physics.

A final discussion of our results will be given in Sec. 5. Finally in the Appendix we list the relevant Feynman rules for the three- and four-particle interactions.

## 2. Effective Lagrangians

### 2.1. Formalism

We are interested in the effects at low energy arising from new physics in the electroweak symmetry-breaking sector. If  $\Lambda$  is the scale above which new physics will manifest itself directly, we want to describe the residual effects on the interactions between the light degrees of freedom of the theory (ie those particles with mass smaller than  $\Lambda$ ) after integrating out the heavy degrees of freedom. In the effective Lagrangian language, these effects are introduced by including in the Lagrangian higher-dimension operators which will be built out of the relevant light degrees of freedom. Since we are interested in new physics associated with the electroweak symmetry-breaking sector, one may expect that the operators involving fermions are suppressed by powers of the fermions masses over the new physics scale and can be neglected (with the possible exception of those associated with the top-quark). Hence in our construction we assume that the fields mostly affected by these residual interactions are the three gauge bosons and the doublet Higgs field which we assume to remain present in the light spectrum and consequently allows us to use a linear<sup>4,5</sup> realization of the  $SU(2)_L \times U(1)_Y$  gauge symmetry. Furthermore we also consider that the new physics respects the parity and charge conjugation symmetries so that operators which violate  $C$  or  $P$  can also be neglected.

In the linear representation of the  $SU(2)_L \times U(1)_Y$  symmetry breaking mechanism, the SM model is the lowest order approximation while the first corrections

which can be built involving bosons are of dimension six and can be written as

$$\mathcal{L}_{\text{eff}} = \sum_n \frac{f_n}{\Lambda^2} \mathcal{O}_n , \quad (1)$$

where the operators  $\mathcal{O}_n$  involve vector boson and/or Higgs boson fields with couplings  $f_n$ . This effective Lagrangian describes well the phenomenology of models that are somehow close to the SM since a light Higgs scalar doublet, which we denote as  $\Phi$ , is still present at low energies. There are eleven possible operators  $\mathcal{O}_n$  that are  $P$  and  $C$  even <sup>4</sup>. The building blocks of the new operators are the covariant derivative

$$D_\mu = \partial_\mu + \frac{i}{2} g' B_\mu + i g \frac{\sigma_a}{2} W_\mu^a , \quad (2)$$

together with the  $U(1)_Y$  and  $SU(2)_L$  field strength tensors  $B_{\mu\nu}$  and  $W_{\mu\nu}^a$ ,

$$\begin{aligned} \hat{B}_{\mu\nu} &= i \frac{g'}{2} B_{\mu\nu} , \\ \hat{W}_{\mu\nu} &= i \frac{g}{2} \sigma^a W_{\mu\nu}^a . \end{aligned} \quad (3)$$

where  $g$  and  $g'$  are the  $SU(2)_L$  and  $U(1)_Y$  coupling constants respectively.

Out of the eleven operators, four of them

$$\begin{aligned} \mathcal{O}_{\Phi,1} &= (D_\mu \Phi)^\dagger \Phi^\dagger \Phi (D^\mu \Phi) , \\ \mathcal{O}_{BW} &= \Phi^\dagger \hat{B}_{\mu\nu} \hat{W}^{\mu\nu} \Phi , \\ \mathcal{O}_{DW} &= \text{Tr} \left( \left[ D_\mu, \hat{W}_{\nu\rho} \right] \left[ D^\mu, \hat{W}^{\nu\rho} \right] \right) , \\ \mathcal{O}_{DB} &= -\frac{g'^2}{2} (\partial_\mu B_{\nu\rho}) (\partial^\mu B^{\nu\rho}) , \end{aligned} \quad (4)$$

affect the gauge-boson two-point functions at tree level when the Higgs field  $\Phi$  is replaced by its VEV

$$\Phi \rightarrow \frac{1}{\sqrt{2}} \begin{pmatrix} 0 \\ v \end{pmatrix} , \quad (5)$$

as we discuss below.

Two of the operators modify only the Higgs self-interactions

$$\begin{aligned} \mathcal{O}_{\Phi,2} &= \frac{1}{2} \partial^\mu (\Phi^\dagger \Phi) \partial_\mu (\Phi^\dagger \Phi) , \\ \mathcal{O}_{\Phi,3} &= \frac{1}{3} (\Phi^\dagger \Phi)^3 , \end{aligned} \quad (6)$$

and they lead to a finite renormalization of the Higgs wave function and the Higgs potential. In this way,  $\mathcal{O}_{\Phi,1}$  and  $\mathcal{O}_{\Phi,2}$  induce a finite wave function renormalization of the Higgs field by a constant  $Z_H^{1/2} = [1 + (f_{\Phi,1} + 2f_{\Phi,2})v^2/2]^{-1/2}$ . This is the only effect of the operator  $\mathcal{O}_{\Phi,2}$  at one loop. Similarly  $\mathcal{O}_{\Phi,3}$  induces a finite renormalization of the Higgs potential.

The five remaining operators:

$$\begin{aligned}
\mathcal{O}_{WWW} &= \text{Tr}[\hat{W}_{\mu\nu}\hat{W}^{\nu\rho}\hat{W}_\rho^\mu], \\
\mathcal{O}_{WW} &= \Phi^\dagger \hat{W}_{\mu\nu} \hat{W}^{\mu\nu} \Phi, \\
\mathcal{O}_{BB} &= \Phi^\dagger \hat{B}_{\mu\nu} \hat{B}^{\mu\nu} \Phi, \\
\mathcal{O}_W &= (D_\mu \Phi)^\dagger \hat{W}^{\mu\nu} (D_\nu \Phi), \\
\mathcal{O}_B &= (D_\mu \Phi)^\dagger \hat{B}^{\mu\nu} (D_\nu \Phi),
\end{aligned} \tag{7}$$

contribute to the gauge–boson three– and four–point functions as well to the Higgs–gauge–boson couplings. In the Appendix we give the corresponding Feynman rules for these vertices. In principle it seems that the operators  $\mathcal{O}_{WW}$  and  $\mathcal{O}_{BB}$  would also modify the triple gauge–boson couplings when the Higgs field is replaced by its VEV (5). However the resulting operators are proportional to the kinetic energy of the  $SU(2)_L$  and  $U(1)_Y$  gauge bosons respectively and therefore they only lead to a finite renormalization of the gauge fields by constants  $Z_{2B}^{1/2} = [1 - f_{BB}v^2/2]^{-1/2}$  and  $Z_{2W}^{1/2} = [1 - f_{WW}v^2/2]^{-1/2}$ .

## 2.2. Low–energy and LEP1 constraints

Some of the operators introduced in the previous section contribute to low–energy observables and their strength can be constrained by precision electroweak measurements. They can affect those measurements through their contributions to both universal<sup>5,16,17</sup> (also called oblique) and non-universal<sup>18,19</sup> (vertex) corrections.

Operators in Eq. (4) modify the oblique corrections to precision electroweak measurements via their contributions at tree level to the transverse components of the gauge–boson propagators. When replacing the Higgs field by its VEV, they lead to the following bilinear gauge boson interactions

$$\begin{aligned}
\mathcal{L} = \frac{1}{2\Lambda^2} \Big\{ & f_{DW} g^2 \vec{W}_{\mu\nu} \partial^2 \vec{W}^{\mu\nu} + f_{DB} g'^2 B_{\mu\nu} \partial^2 B^{\mu\nu} + \\
& f_{BW} m_Z^2 s c W_{\mu\nu}^3 B^{\mu\nu} + f_{\Phi,1} \frac{v^2}{2} m_Z^2 Z^\mu Z_\mu \Big\}, \tag{8}
\end{aligned}$$

where  $s = \sin \theta_W$  and  $c = \cos \theta_W$ . This contribution to the oblique corrections can be parametrized in terms of seven parameters<sup>5,17</sup>, the usual  $S$ ,  $T$ , and  $U$  (or  $\epsilon_1$ ,  $\epsilon_2$ ,  $\epsilon_3$ )<sup>20</sup> together with four running form factors, such as, for instance, the running of  $\alpha_{QED}$ . From Eq. (8) one can see that  $\mathcal{O}_{\Phi,1}$  modifies the  $Z$  mass but not the  $W$  mass what gives a contribution to the  $\rho = \alpha T = \epsilon_1$  parameter.  $\mathcal{O}_{BW}$  induces a mixing between  $B$  and  $W^3$  and contributes to the  $S$  (*i.e.*  $\epsilon_3$ ) parameter.  $\mathcal{O}_{DW}$  and  $\mathcal{O}_{DB}$  contribute to the running charges and they lead for instance to an anomalous running of  $\alpha_{QED}$  and the weak mixing angle.

Combining the information from precision measurements both at the  $Z$ –pole as well as at low energy it is possible to constrain unambiguously the values of the coefficients of the operators (4). We present here the results from a recent analysis (second article in<sup>17</sup>). The exact limits depend on the values of  $m_H$  and

$m_{\text{top}}$  as the SM prediction depends on those masses. For  $m_{\text{top}} = 175$  GeV and  $90 \text{ GeV} \leq m_H \leq 800 \text{ GeV}$  they obtain the following 95% allowed intervals (in units of  $\text{TeV}^{-2}$ )

$$\begin{aligned} -1.2 &\leq f_{DW}/\Lambda^2 \leq 0.56 , \\ -33.6 &\leq f_{DB}/\Lambda^2 \leq 5.6 , \\ -1. &\leq f_{BW}/\Lambda^2 \leq 8.6 , \\ -0.07 &\leq f_{\Phi,1}/\Lambda^2 \leq 0.61 . \end{aligned} \tag{9}$$

These constraints are severe enough to make it very difficult to observe the effect of these operators in the high-energy observables discussed later. In what follows we will neglect their effect in our studies.

The five operators in Eq. (7), also denoted as “blind”, do not give tree-level contributions to the low-energy electroweak precision data. They enter however via one-loop contributions, which, although generally suppressed by a factor of  $1/16\pi^2$  relative to tree-level effects, can still be large enough to lead to measurable effects which allows to impose bounds on the corresponding coefficients. These bounds, however, are far from unambiguous. One must bear in mind that without a particular model it is impossible to predict the interference between the tree-level and the loop-level corrections as well as possible cancellation among the different one-loop contributions. The limits presented here (from the analysis in Ref. <sup>17</sup>) are obtained under the “naturalness” assumption that large such cancellation do not occur. In this way, considering only the effect of one operator at a time, one has the following constraints at 95% CL (in units of  $\text{TeV}^{-2}$ )

$$\begin{aligned} -15 &\leq f_{WW}/\Lambda^2 \leq 25 , \\ -12. &\leq f_W/\Lambda^2 \leq 2.5 , \\ -7.6 &\leq f_B/\Lambda^2 \leq 22 , \\ -24 &\leq f_{WW}/\Lambda^2 \leq 14 , \\ -79 &\leq f_{BB}/\Lambda^2 \leq 47 . \end{aligned} \tag{10}$$

These limits depend in a complicated way on the Higgs mass. The values quoted above are valid for  $m_H = 200 \text{ GeV}$ .

### 2.3. Constraints from gauge-boson production

Some of the operators introduced in Sec. 2.1 contribute the triple gauge-boson self-couplings and they can be constrained by the direct measurements of vector boson pair production processes that have been conducted by the CDF and D Collaborations <sup>21</sup> at the Fermilab Tevatron and by the four LEP <sup>22</sup> experiments at CERN.

The general form of the  $VW^+W^-$  vertices ( $V = Z, \gamma$ ) in the presence of the effective Lagrangian (1) can be found in the Appendix. It involves the coefficients  $f_W$ ,  $f_B$ ,  $f_{WW}$  and  $f_{DW}$ . When neglecting the contribution from “not-blind”

operators ( $f_{DW} = 0$ ) the triple gauge–boson effective interaction can be rewritten as the can be rewritten as the standard parametrization <sup>23</sup>:

$$\begin{aligned} \mathcal{L}_{WWV} = & -ig_{WWV} \left\{ g_1^V \left( W_{\mu\nu}^+ W^{-\mu} V^\nu - W_\mu^+ V_\nu W^{-\mu\nu} \right) \right. \\ & \left. + \kappa_V W_\mu^+ W_\nu^- V^{\mu\nu} + \frac{\lambda_V}{m_W^2} W_{\mu\nu}^+ W^{-\nu\rho} V_\rho^\mu \right\}, \end{aligned} \quad (11)$$

where  $g_{WW\gamma} = e$ ,  $g_{WWZ} = e/(s c)$ . In general these vertices involve six dimensionless couplings  $g_1^V$ ,  $\kappa_V$ , and  $\lambda_V$  ( $V = \gamma$  or  $Z$ ), after imposing  $C$  and  $P$  invariance. Electromagnetic gauge invariance requires that  $g_1^\gamma = 1$ , while the other five couplings are related to the new operators according to:

$$\begin{aligned} \Delta g_1^Z &= g_1^Z - 1 = \frac{1}{2} \frac{m_Z^2}{\Lambda^2} f_W, \\ \Delta \kappa_\gamma &= \kappa_\gamma - 1 = 1 + \frac{1}{2} \frac{m_W^2}{\Lambda^2} (f_W + f_B), \end{aligned} \quad (12)$$

$$\begin{aligned} \Delta \kappa_Z &= \kappa_Z - 1 = 1 + \frac{1}{2} \frac{m_Z^2}{\Lambda^2} (c^2 f_W - c^2 f_B), \\ \lambda_\gamma &= \lambda_Z = \frac{3g^2 m_W^2}{2\Lambda^2} f_{WWW}. \end{aligned} \quad (13)$$

In this case only three of the five couplings remain independent <sup>5</sup> which can be chosen to be  $\Delta \kappa_\gamma$ ,  $\lambda_\gamma$ , and  $\Delta g_1^Z$ . The remaining  $WWZ$  coupling parameters  $\lambda_Z$  and  $\Delta \kappa_Z$  are determined by the relations <sup>5</sup>

$$\lambda_Z = \lambda_\gamma \quad \Delta \kappa_Z = -\Delta \kappa_\gamma \tan^2 \theta_W + \Delta g_1^Z. \quad (14)$$

A different set of parameters has also been used by the LEP Collaborations <sup>24</sup> in terms of three independent couplings,  $\alpha_{B\Phi}$ ,  $\alpha_{W\Phi}$ , and  $\alpha_W$  which simply correspond to the coefficients of the  $\mathcal{O}_B$ ,  $\mathcal{O}_W$ , and  $\mathcal{O}_{WWW}$  operators but defined with a different normalization than the  $f_i$  coefficients. With that normalization these parameters are related to the parametrization (11) through  $\Delta \kappa_\gamma = \alpha_{B\Phi} + \alpha_{W\Phi}$ ,  $\Delta g_1^Z = \alpha_{W\Phi}/c_W^2$ , and  $\alpha_W = \lambda_\gamma$  while  $\lambda_Z$  and  $\Delta \kappa_Z$  are determined by the relations (14).

LEP experiments are sensitive to anomalous triple gauge coupling through the  $W$ -pair cross section, the angular distribution of the produced  $W$ 's and their helicity components which are deduced from the angles of the  $W$  decay products. In addition single  $W$  and single  $\gamma$  production are also sensitive to the  $WW\gamma$  vertex.

Triple gauge–boson couplings measurements at DØ are based on the analysis of di–boson production events. They obtain limits on  $WW\gamma$  from a fit to the photon  $E_T$  spectrum in  $W\gamma$  with the subsequent decay  $W \rightarrow l\nu$ . Limits on  $WWZ$  and  $WW\gamma$  couplings are obtained from a fit to the  $E_T$  of the two charged leptons in  $p\bar{p} \rightarrow W^+W^-X \rightarrow l\nu l'\nu'X$  events and from a fit to the  $p_T$  spectrum of the electron–neutrino system in  $p\bar{p} \rightarrow W^+W^-$  (or  $W^\pm Z$ )  $X \rightarrow l\nu jj$ .

The enhancement of the gauge–boson–pair cross section from anomalous couplings increases with the center-of-mass energy, which in principle gives larger sensitivity to Tevatron experiments compared with LEP. However, since the backgrounds are also larger at Tevatron, the overall sensitivity is similar to that of the LEP experiments. The published results from  $D\bar{O}$  and the four LEP experiments were combined to produce the tightest available  $WW\gamma$  and  $WWZ$  coupling limits<sup>25</sup>. The 95% CL limits presented in this analysis are

$$\begin{aligned} -0.15 &\leq \Delta\kappa_\gamma \leq 0.41 \quad \text{for } \lambda_\gamma = 0, \\ -0.16 &\leq \lambda_\gamma \leq 0.10 \quad \text{for } \Delta\kappa_\gamma = 0, \end{aligned} \quad (15)$$

which translates into the following bounds on the coefficients of the higher–dimension operators in  $(\text{TeV})^{-2}$ :

$$\begin{aligned} -46 &\leq (f_W + f_B)/\Lambda^2 \leq 127 \quad \text{for } f_{WW} = 0, \\ -41 &\leq f_{WW}/\Lambda^2 \leq 26 \quad \text{for } f_W + f_B = 0. \end{aligned} \quad (16)$$

Notice that, since neither  $f_{WW}$  nor  $f_{BB}$  contribute to the triple gauge–boson vertices, no direct constraint on these couplings can be derived from this analysis. Their first contribution is a modification of the Higgs couplings which leads to the effects we are going to discuss next.

### 3. Higgs Physics

#### 3.1. Couplings

Four of the "blind" operators in Eq. (7),  $\mathcal{O}_{WW}$ ,  $\mathcal{O}_{BB}$ ,  $\mathcal{O}_W$ , and  $\mathcal{O}_B$ , also induce anomalous  $H\gamma\gamma$ ,  $HZ\gamma$ ,  $HZZ$  and  $HWW$  couplings, which, in the unitary gauge, are given by

$$\begin{aligned} \mathcal{L}_{\text{eff}}^H &= g_{H\gamma\gamma} H A_{\mu\nu} A^{\mu\nu} + g_{HZ\gamma}^{(1)} A_{\mu\nu} Z^\mu \partial^\nu H \\ &+ g_{HZ\gamma}^{(2)} H A_{\mu\nu} Z^{\mu\nu} + g_{HZZ}^{(1)} Z_{\mu\nu} Z^\mu \partial^\nu H \\ &+ g_{HZZ}^{(2)} H Z_{\mu\nu} Z^{\mu\nu} + g_{HWW}^{(2)} H W_{\mu\nu}^+ W_-^{\mu\nu} \\ &+ g_{HWW}^{(1)} (W_{\mu\nu}^+ W_-^\mu \partial^\nu H + \text{h.c.}), \end{aligned} \quad (17)$$

where  $A(Z)_{\mu\nu} = \partial_\mu A(Z)_\nu - \partial_\nu A(Z)_\mu$ . The effective couplings  $g_{H\gamma\gamma}$ ,  $g_{HZ\gamma}^{(1,2)}$ , and  $g_{HZZ}^{(1,2)}$  and  $g_{HWW}^{(1,2)}$  are related to the coefficients of the operators appearing in Eq. (7) through,

$$\begin{aligned} g_{H\gamma\gamma} &= -\left(\frac{gm_W}{\Lambda^2}\right) \frac{s^2(f_{BB} + f_{WW})}{2}, \\ g_{HZ\gamma}^{(1)} &= \left(\frac{gm_W}{\Lambda^2}\right) \frac{s(f_W - f_B)}{2c}, \\ g_{HZ\gamma}^{(2)} &= \left(\frac{gm_W}{\Lambda^2}\right) \frac{s[s^2 f_{BB} - c^2 f_{WW}]}{c}, \end{aligned} \quad (18)$$



$$\begin{aligned}
g_{HZZ}^{(1)} &= \left( \frac{gm_W}{\Lambda^2} \right) \frac{c^2 f_W + s^2 f_B}{2c^2} , \\
g_{HZZ}^{(2)} &= - \left( \frac{gm_W}{\Lambda^2} \right) \frac{s^4 f_{BB} + c^4 f_{WW}}{2c^2} , \\
g_{HWW}^{(1)} &= \left( \frac{gm_W}{\Lambda^2} \right) \frac{f_W}{2} , \\
g_{HWW}^{(2)} &= - \left( \frac{gm_W}{\Lambda^2} \right) f_{WW} .
\end{aligned}$$

Notice that, unlike in the SM, the  $HZZ$  and  $HWW$  couplings are not proportional to each other as a consequence of the presence of the operators  $\mathcal{O}_B$  and  $\mathcal{O}_{BB}$  which involve the  $U(1)_Y$  strength tensor. In what follows we will discuss the effects of the new Higgs couplings in Eq. (17) on the expected Higgs signals and how existing data can be used to further constraint the values of the coefficients of these anomalous operators.

### 3.2. Decay modes

Higgs decays into gauge bosons are affected by the presence of the higher-dimension operators and this will affect its signature in colliders. Larger relative effects are expected in the decays  $H \rightarrow \gamma\gamma$  and  $H \rightarrow Z\gamma$  which in the SM occur only at the one-loop level with contributions from loops with any massive particle in the loop. However, the existence of the new interactions (17) can enhance these widths in a significant way as they contribute at tree level. These decay widths are given by:

$$\Gamma(H \rightarrow \gamma\gamma) = \frac{m_H^3}{4\pi} \left| g_{H\gamma\gamma} + \frac{\alpha}{8\pi v} I \right|^2 , \quad (19)$$

where  $v$  is the Higgs VEV (5) and  $I$  is the complex form factor for the SM contribution to the width<sup>26,27</sup> from loops of all particles with spin  $i$ , charge  $e_i$  and colour factor  $N_{ci}$ ,  $I = \sum_i N_{ci} e_i^2 F_i$ .  $F$  is a complex function which depends on mass and spin of the particle running in the loop. Defining  $\tau = 4m_i^2/m_H^2$

$$\begin{aligned}
F_1 &= 2 + 3\tau + 3\tau(2 - \tau)f(\tau) , \\
F_{1/2} &= -2\tau[1 + (1 - \tau)f(\tau)] , \\
F_0 &= \tau(1 - \tau f(\tau)) .
\end{aligned} \quad (20)$$

where

$$f(\tau) = \begin{cases} \left[ \sin^{-1}(\sqrt{1/\tau}) \right]^2 & \text{for } \tau \geq 1 , \\ \frac{1}{4} \left[ \ln \left( \frac{1+\sqrt{1-\tau}}{1-\sqrt{1-\tau}} \right) - i\pi \right]^2 & \text{for } \tau \leq 1 . \end{cases} \quad (21)$$

The larger contribution to the SM form factor  $I$  comes from the  $W$  and the top-quark loops being the  $W$  contribution larger by at least a factor 4 for  $m_H > 100$  GeV. We can see from Eq. (19) that the anomalous contribution is of the order of

the SM one for  $g_{H\gamma\gamma} \sim \frac{\alpha}{8\pi v}$  ( $f/\Lambda^2 \sim \mathcal{O}(\text{TeV}^{-2})$ ).

$$\Gamma(H \rightarrow \gamma Z) = \frac{m_H^3}{16\pi} \left(1 - \frac{x_Z}{4}\right)^3 \left| g_{HZ\gamma}^{(1)} + 2g_{HZ\gamma}^{(2)} + \frac{\alpha}{2\sqrt{2}\pi v} A \right|^2, \quad (22)$$

where  $x_Z = 4m_Z^2/m_H^2$  and  $A$  is the form factor for the SM contribution to the width  $A = A_F + A_W$  where  $A_W$  gives the contribution from  $W$  loops and  $A_F$  from fermion loops, which is dominated by the top-quark loop, and the explicit form can be found in Eq. (2.21) of Ref. <sup>27</sup>. The value of  $A_F$  is small compared to  $A_W$  ( $|A_W|/|A_F| > 10$  for  $m_H < 300$  GeV).

In Fig. 1 we plot the decay widths for these processes as a function of the anomalous coefficients and in Fig. 2 the corresponding branching ratios as a function of the Higgs mass for several values of the anomalous coefficients. From the figures we see that the branching fractions to these decay modes are enhanced by 2–4 orders of magnitude as compared to the SM and they can become dominant for Higgs masses below  $W$ -pair production threshold. Moreover for larger values of  $f/\Lambda^2$  they are still a relevant decay mode even above  $W$ -pair production threshold.

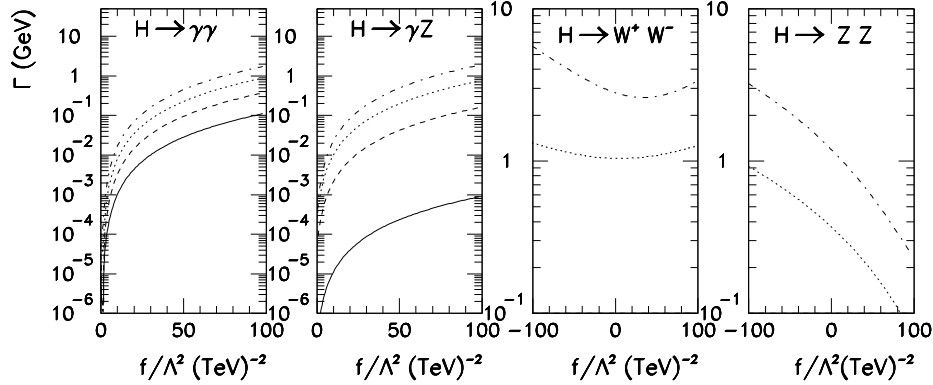


Fig. 1. Higgs boson decay widths for the different channels as a function of the anomalous couplings assuming  $f_{WW} = f_{BB} = f_W = f_B = f$  while all others are set to zero. The curves correspond to different Higgs boson mass:  $m_H = 100, 150, 200, 250$  GeV for solid, dashed, dotted and dot-dashed respectively.

It is important to notice that the decay mode  $H \rightarrow \gamma\gamma$  only depends on the values of  $f_{WW}$  and  $f_{BB}$  which are the “blind” operators which do not contribute the triple gauge-boson vertices. Therefore, it is possible to have significant enhancements of this decay mode without conflicting with the existing bounds on anomalous gauge-boson couplings presented in Sec. 2.3. Conversely, this enhancement, can be used to search for the Higgs boson in  $\gamma\gamma$  signatures, which are cleaner at hadron colliders. In Sec. 4 we will make use of this enhancement in order to place bounds on the  $f/\Lambda^2$  coefficients from existing data from the Tevatron and LEP II experiments.

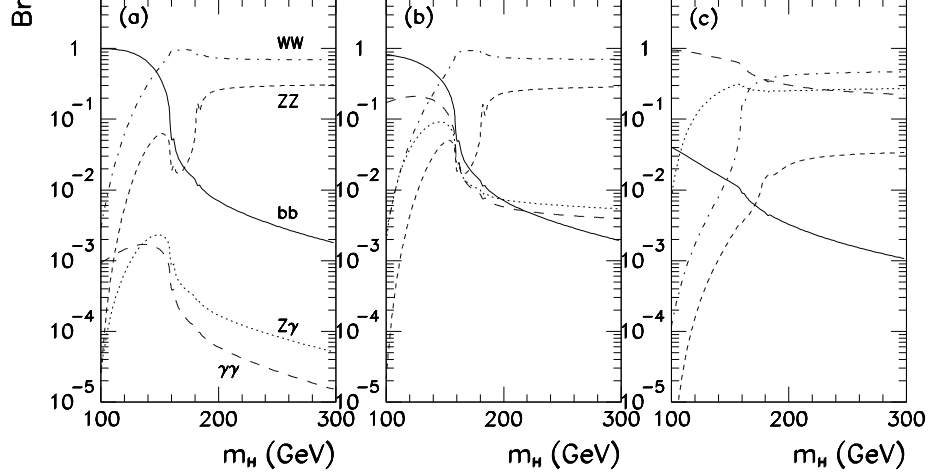


Fig. 2. Higgs boson decay branching fractions for the different channels as a function of Higgs mass for different value of the anomalous coupling  $f_{WW} = f_{BB} = f_W = f_B = f$  while all others are set to zero: (a) SM ( $f = 0$ ), (b)  $f/\Lambda^2 = 10 \text{ TeV}^{-2}$ , and (c)  $f/\Lambda^2 = 100 \text{ TeV}^{-2}$ .

The decay modes into weak-boson pairs,  $H \rightarrow ZZ$  and  $H \rightarrow W^+W^-$  have tree-level contributions from the SM and therefore the effect of the higher-dimension operators is large only for large values of the coefficients. The width for these decay modes can be written as:

$$\Gamma(H \rightarrow ZZ) = \frac{m_H^3}{32\pi} \sqrt{1 - x_Z} \left\{ 2 \left[ \frac{x_Z}{2v} + (x_Z - 2)g_{HZZ}^{(2)} - g_{HZZ}^{(1)} \right]^2 + \left[ \frac{1}{v} - x_Z \left( \frac{1}{2v} + g_{HZZ}^{(2)} \right) - g_{HZZ}^{(1)} \right]^2 \right\}, \quad (23)$$

$$\Gamma(H \rightarrow W^+W^-) = \frac{m_H^3}{16\pi} \sqrt{1 - x_W} \left\{ 2 \left[ \frac{x_W}{2v} + \left( \frac{x_W}{2} - 1 \right) g_{HWW}^{(2)} - g_{HWW}^{(1)} \right]^2 + \left[ \frac{1}{v} - \frac{x_W}{2} \left( \frac{1}{v} + g_{HWW}^{(2)} \right) - g_{HWW}^{(1)} \right]^2 \right\}. \quad (24)$$

where  $x_Z = 4m_Z^2/m_H^2$  and  $x_W = 4m_W^2/m_H^2$ . In these expressions the first term in square brackets corresponds to the decay into transversely polarized gauge bosons while the second corresponds to decay into longitudinally polarized ones. We can see from Eq. (23) that the anomalous contribution to these widths is of the order of the SM one for  $g_{HZZ} \sim \frac{1}{v}$  what implies  $f/\Lambda^2 \sim 100 \text{ TeV}^{-2}$ .

In Fig. 1 we plot the decay widths for these modes as a function of the anomalous coefficients and in Fig. 2 the corresponding branching ratios as a function of the Higgs mass for several values of the anomalous coefficients. As expected the effect in the  $W^+W^-$  decay mode is at most a factor two even for very large values of the

$f$  coefficients and the relative effect increases with  $m_H$ . The effect is a bit larger for the decay  $H \rightarrow ZZ$ .

### 3.3. Production mechanisms at $p\bar{p}$ and $e^+e^-$ collisions

Since the Higgs couplings to light fermions, which are the dominant component of the initial state at  $e^+e^-$  and hadron colliders, are very weak, the production cross sections for the Higgs boson at colliders are in general small. In the SM, production mechanisms with largest cross sections are those where the Higgs couples to an intermediate heavy particle either a weak gauge bosons or the top-quark.

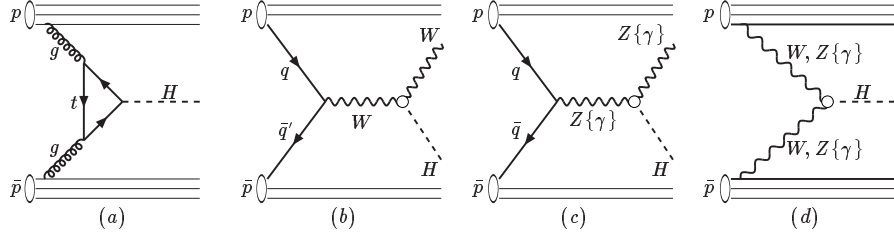


Fig. 3. Dominant Higgs production mechanisms at hadron colliders: **(a)** gluon fusion, **(b)** associated Higgs- $W$  production, **(c)** associated Higgs- $Z$  production (also anomalous Higgs- $\gamma$ ), and **(d)** gauge-boson fusion. We denote by a white circle those vertices that are modified in the presence of the anomalous Higgs couplings (17) and by a particle between brackets those particles whose contributions only arise for non-vanishing anomalous couplings.

In Fig. 3 we display the dominant production mechanisms for the Higgs boson at hadron colliders. For the SM Higgs they are: (a) gluon fusion where two initial gluons from the hadrons couple to the Higgs boson at one-loop via a virtual top-quark loop, (b) associated Higgs production with a  $W$  or (c) a  $Z$  boson, and (d)  $W^+W^-$  or  $ZZ$  fusion. In Fig. 4 we plot the cross sections for these processes at the Tevatron center-of-mass energy of  $\sqrt{s} = 1.8$  GeV<sup>28</sup> as a function of the Higgs boson mass. As seen in Fig. 4, the production mechanism with largest cross section is gluon fusion. However, as we have discussed before (see Fig. 2.a) in the SM the light Higgs boson decays dominantly to  $b$ -quarks and in consequence the gluon-fusion process is swamped by the QCD background of  $b$ -quark-pair production since there is no other particle in the final state which could be used to tag the event. As we have seen in the previous section the presence of the new operators modify the Higgs decay modes and the Higgs may decay dominantly into photons. However, still in this case, gluon-fusion production is swamped by the two-photon background from QED.

The most important production mechanism for a SM Higgs at the Tevatron is associated production of the Higgs boson with a  $W$  or a  $Z$  whose decay products can be used to trigger the event. On the other hand, the gauge-boson-fusion processes (d) has similar problems to the gluon fusion, as it leads to final states

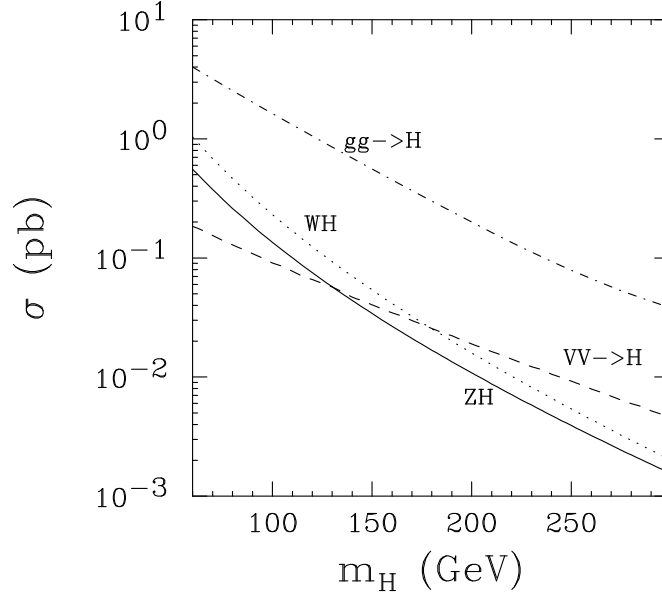


Fig. 4. Higgs production cross sections at the Fermilab Tevatron as a function of the Higgs mass in the SM. The curves correspond to different production processes as labeled in the figure.

with two high-rapidity jets from the proton remanent plus two b-jets from the Higgs decay and it is also well below the corresponding QCD background. As we will see in Sec. 4.2 in the presence of the new operators gauge-boson fusion can give a significant contribution to the process  $p\bar{p} \rightarrow jj\gamma\gamma$ .

The operators (7) induce new couplings between the Higgs and the gauge bosons and in consequence modify the SM production processes cross section by giving rise to new contributions to the SM amplitudes  $q\bar{q} \rightarrow Z^*(W^*) \rightarrow Z(W)H$  as well as new amplitudes such as  $q\bar{q} \rightarrow \gamma^* \rightarrow ZH$ . They also provide new production mechanisms such as associated production of the Higgs boson with a photon (See Fig. 3.c),  $q\bar{q} \rightarrow Z^*, \gamma^* \rightarrow \gamma H$  which can occur via  $g_{H\gamma\gamma}$  as well as  $g_{HZ\gamma}^{(1)}$  and  $g_{HZ\gamma}^{(2)}$ . Higgs production by gauge-boson fusion is also modified as now also  $Z\gamma$  and  $\gamma\gamma$  fusion are possible (See Fig. 3.d).

In Fig. 5 we plot the Higgs production cross section for the associated production processes in the presence of the new operators. For the purpose of illustration we assume all the four coefficients equal  $f_{WW} = f_{BB} = f_W = f_B = f$ . As seen in Fig. 5, for large values of the anomalous coefficients, the presence of the new operators yields production rates larger than in the SM. However for intermediate values, the associated Higgs- $Z$  and Higgs- $W$  production cross sections can be smaller than in the SM as a consequence of the possible destructive interference between the SM amplitudes and some of the anomalous ones as seen in the left panel in Fig. 5. We also see that associated Higgs- $\gamma$  production is particularly dominant for Higgs bosons lighter than the  $Z$  when an on-shell  $Z$  can decay into  $\gamma H$ .

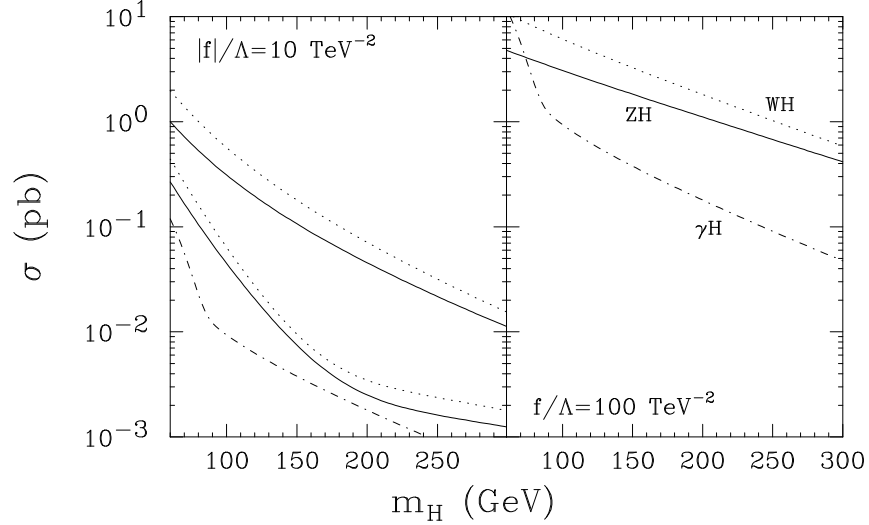


Fig. 5. Associated Higgs production cross sections at the Fermilab Tevatron as a function of the Higgs mass in the presence of anomalous couplings. The left figure corresponds to  $f_{WW} = f_{BB} = f_W = f_B = f$  with  $|f| = 10 \text{ TeV}^{-2}$ . The two upper curves are for  $ZH$  and  $WH$  productions for  $f = -10 \text{ TeV}^{-2}$  while the lower ones are for  $f = 10 \text{ TeV}^{-2}$ . The associated  $\gamma H$  cross section (dash-dotted) line is practically independent on the sign of  $f$ . The right figure corresponds to  $f = 100 \text{ TeV}^{-2}$ .

At  $e^+e^-$  collisions the dominant production mechanism for the SM Higgs are associated Higgs- $Z$  production (also known as “Higgs-strahlung”),  $e^+e^- \rightarrow ZH$ , and  $W^+W^-$  fusion  $e^+e^- \rightarrow \nu_e \bar{\nu}_e H$ . At the LEP II energies the gauge-fusion process has a considerably smaller cross section as it is suppressed by an additional power of the electroweak coupling constant.

The operators (7) give rise to new contributions to the SM amplitude for Higgs- $Z$  production as well as new amplitudes:  $e^+e^- \rightarrow Z^* \gamma^* \rightarrow ZH$ . They also provide the possibility of associated production of the Higgs boson with a photon,  $e^+e^- \rightarrow Z^*, \gamma^* \rightarrow \gamma H$ . In Fig. 6 we plot the cross sections for these processes at the center-of-mass energy  $\sqrt{s} = 190 \text{ GeV}$ . Again we see that for intermediate values of the anomalous coupling  $f$ , the production cross section for Higgs- $Z$  can be smaller than in the SM as a consequence of the negative interference between the SM and the anomalous amplitudes. For large values of the coupling, however the cross section is always larger than in the SM.

## 4. Study of Specific Processes

### 4.1. Introduction

In this section we are going to analyze some processes which can be used to study the effect of the dimension-six operators in Higgs searches. The aim is to illustrate

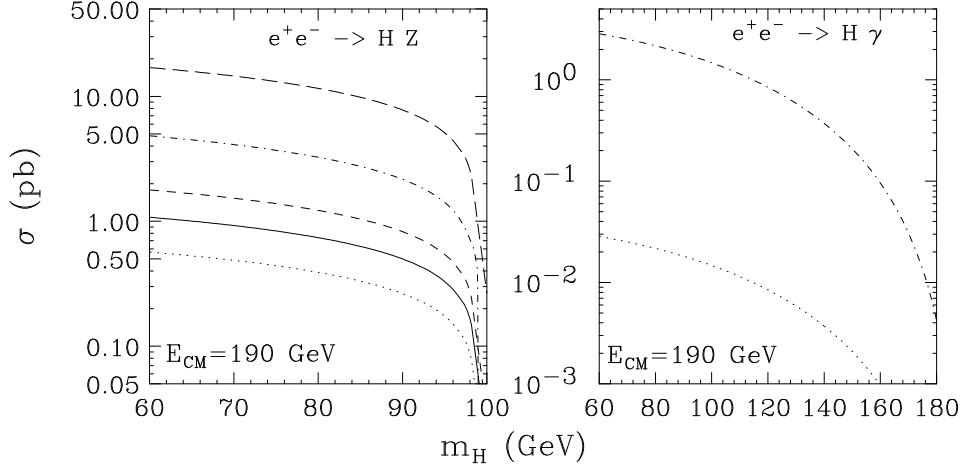


Fig. 6. Higgs production cross sections at LEP II as a function of the Higgs mass. The curves correspond to different values of the anomalous couplings assuming  $f_{WW} = f_{BB} = f_W = f_B = f = 0, 10, -10, 100, -100 \text{ TeV}^{-2}$  for solid, dotted dashed, dash-dotted, and long-dashed respectively. Notice that for  $e^+e^- \rightarrow \gamma H$  the cross section is almost independent of the sign of the anomalous coupling and we are plotting the cross section only for positive values:  $f/\Lambda^2 = 10(100) \text{ TeV}^{-2}$  for dash (dash-dotted).

how by using data already collected by the experiments at Tevatron and LEP II it is possible to obtain further constraints on the values of the coefficients of the operators (7). In Sec. 4.6 we will show the final results of the combination of all these searches and compare them with the limits discussed in Sec. 2.3.

We first consider Higgs production at the Fermilab Tevatron and CERN LEP II collider with its subsequent decay into two photons. We explore the signatures:

$$\begin{aligned}
 p\bar{p} &\rightarrow jj\gamma\gamma, \\
 p\bar{p} &\rightarrow \gamma\gamma + \cancel{E}_T, \\
 p\bar{p} &\rightarrow \gamma\gamma\gamma, \\
 e^+e^- &\rightarrow \gamma\gamma\gamma.
 \end{aligned}
 \tag{25}$$

This type of events containing two photons plus missing energy, additional photons or charged fermions represent a signature for several theories involving physics beyond the SM, such as some classes of supersymmetric models<sup>29</sup> and they have been extensively searched for<sup>30,31,32,33</sup>. In the framework of anomalous Higgs couplings presented before, they can also arise from the production of a Higgs boson which subsequently decays in two photons. As we have seen in Sec. 3.2 in the SM, the decay width  $H \rightarrow \gamma\gamma$  is very small since it occurs just at one-loop level<sup>26</sup>. However, the existence of the new interactions (17) can enhance this width in a significant way. Recent analyses of these signatures presented a good agreement with the expectations from the SM. Thus we can employ these negative experimental results to constrain new anomalous couplings in the bosonic sector of the SM. We will also

discuss the expected sensitivity at the Tevatron collider with increased luminosity as well as in the Next Linear Collider (NLC).

In the calculations presented below, we have included all SM (QCD plus electroweak), and anomalous contributions that lead to these final states. The SM one-loop contributions to the  $H\gamma\gamma$  and  $HZ\gamma$  vertices are introduced through the use of the effective operators with the corresponding form factors (20) and (22) in the coupling. Neither the narrow-width approximation for the Higgs boson contributions, nor the effective- $W$ -boson approximation were employed. In this way, the effect of all interferences between the anomalous signature and the SM background has been consistently included. The SM Feynman diagrams corresponding to the background subprocess can be generated by Madgraph<sup>34</sup> in the framework of Helas<sup>35</sup>. The anomalous couplings arising from the Lagrangian (1) were implemented in Fortran routines and were included accordingly. For calculations of processes at the Tevatron, we have used the MRS (G)<sup>36</sup> set of proton structure functions with the scale  $Q^2 = \hat{s}$ .

In order to compare the theoretical predictions with the experimental results from the different searches described below, one must compute the expected number of events after including the experimental cuts on the final state particles. Some of the cuts take into account the geometrical acceptance of the detector and others are designed to improve the sensitivity to the signal while reducing the possible backgrounds. The cuts employed in this review are usually defined in terms of the following kinematical variables

pseudorapidity	$\eta = -\ln \frac{\theta}{2}$	
transverse momentum	$p_T = \sqrt{E^2 - m^2 - p_L^2}$	
transverse mass	$E_T = \sqrt{E^2 - p_L^2}$	(26)
invariant mass of the system $ab$	$M_{ab}^2 = (p_a + p_b)^2$	
separation between $a$ and $b$	$\Delta R_{ab} = \sqrt{(\eta_a - \eta_b)^2 + (\phi_a - \phi_b)^2}$	

where  $p_a$  is the four-momentum of particle  $a$ ,  $E$  is the particle energy,  $p_L$  is the projection of the particle three-momentum along the beam axis,  $\theta$  is polar the scattering angle,  $\tan \theta = p_T/p_L$ , and  $\phi$  is the azimuthal angle of the momentum.

The coupling  $H\gamma\gamma$  derived in (18) involves  $f_{WW}$  and  $f_{BB}$ <sup>6</sup>. In consequence, the anomalous signature for any of the processes in Eq. (25) is only possible when those couplings are not vanishing. The couplings  $f_B$  and  $f_W$ , on the other hand, affect the production mechanisms for the Higgs boson. In what follows, we are going to present the results of the analysis of the processes (25) for two different scenarios of the anomalous coefficients:

- (i) Suppressed  $VVV$  couplings compared to the  $H\gamma\gamma$  vertex:  $f_{BB,WW} \gg f_{B,W}$ ,
- (ii) All coupling with the same magnitude:  $f_{BB,WW,B,W} = f$ .



In order to establish the attainable bounds on the coefficients, an upper limit on the number of signal events based on Poisson statistics is imposed. In the absence of background this implies  $N_{\text{signal}} < 1$  (3) at 64% (95%) CL. In the presence of background events, the modified Poisson analysis <sup>37</sup> was employed.

#### 4.2. $p\bar{p} \rightarrow jj\gamma\gamma$

Let us start with the analysis of the process  $p\bar{p} \rightarrow jj\gamma\gamma$ . A total of 1928 SM amplitudes are involved in the different subprocesses contributing to this signature <sup>38</sup> while 236 anomalous amplitudes <sup>12</sup> are generated by the operators (7). All these amplitudes are computed numerically as described above. The dominant anomalous contribution to this final state when the two photons have large invariant mass arises from Higgs- $V$  (where  $V$  is any of the gauge boson) associated production and from gauge-boson fusion and are displayed in Fig. 7.

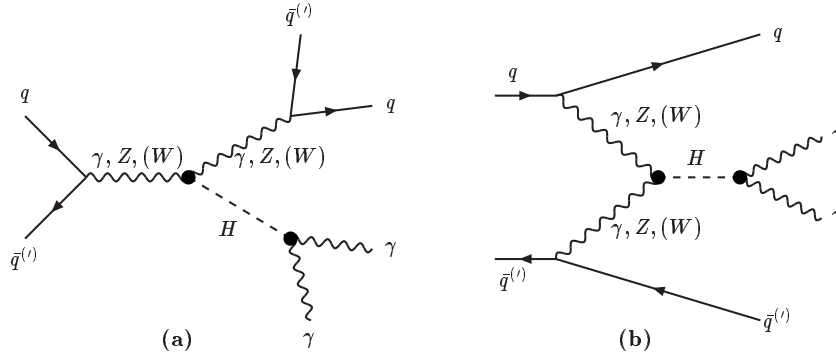


Fig. 7. Dominant anomalous contribution for the  $\gamma\gamma jj$  production: (a) Associated production, (b) Gauge-boson fusion.

The DØ Collaboration at the Fermilab Tevatron have searched for  $p\bar{p} \rightarrow \gamma\gamma jj$  events with high two-photon invariant masses <sup>31</sup> using the  $100 \text{ pb}^{-1}$  of integrated luminosity collected in Run I. They report that no event with two-photon invariant mass in the range  $60 < M_{\gamma\gamma} < 220$  was observed. In order to use this DØ result one must compute the expected number of events in the presence of the anomalous coefficients after including the same cuts on the final state particles which take into account the geometrical acceptance of the detector and which are also aimed to

maximally reduce the possible backgrounds as discussed below:

$$\begin{aligned}
&\text{For the photons} \\
&|\eta_{\gamma 1}| < 1.1 \text{ or } 1.5 < |\eta_{\gamma 1}| < 2 \quad p_T^{\gamma 1} > 20 \text{ GeV} \\
&|\eta_{\gamma 2}| < 1.1 \text{ or } 1.5 < |\eta_{\gamma 2}| < 2.25 \quad p_T^{\gamma 2} > 25 \text{ GeV} \\
&\sum \vec{p}_T^\gamma > 10 \text{ GeV} \\
&\text{For the jets} \\
&|\eta_{j1}| < 2 \quad p_T^{j1} > 20 \text{ GeV} \\
&|\eta_{j2}| < 2.25 \quad p_T^{j2} > 15 \text{ GeV} \\
&\sum \vec{p}_T^j > 10 \text{ GeV} \quad R_{\gamma j} > 0.7 \\
&40 \leq M_{jj} \leq 150 \text{ GeV}
\end{aligned} \tag{27}$$

Since we are not working in the narrow width approximation we must also impose the reconstruction of the photon invariant mass around the Higgs mass. In order to do so we assume an invariant-mass resolution for the two photons of  $\Delta M_{\gamma\gamma}/M_{\gamma\gamma} = 0.15/\sqrt{M_{\gamma\gamma}} \oplus 0.007$ <sup>28</sup>. Both signal and background were integrated over an invariant-mass bin of  $\pm 2\Delta M_{\gamma\gamma}$  centered around  $m_H$ .

As mentioned above the anomalous signature receives contributions from both Higgs associated production and gauge-boson fusion. For the sake of illustration, we show in Fig. 8.a the invariant mass distribution of the two photons for  $m_H = 70$  GeV and  $f_{BB}/\Lambda^2 = 100 \text{ TeV}^{-2}$ , without any cut on  $M_{\gamma\gamma}$  or  $M_{jj}$ . We see a peak of events due to the on-shell Higgs production. Figure. 8.b displays the invariant mass distribution of the jet pair after imposing the Higgs mass reconstruction on the  $\gamma\text{--}\gamma$  system. One can clearly see that there is a significant excess of events in the region  $M_{jj} \sim m_{W,Z}$  corresponding to the process of associate production (Fig.7.a). It is also possible to distinguish the tail corresponding to the Higgs production from  $WW/ZZ$  fusion (Fig.7.b) for  $M_{jj} > 100$  GeV. One can isolate the majority of events due to associated production, and the corresponding background, by integrating over a bin centered on the  $W$  or  $Z$  mass, which is equivalent to the two-jets-invariant-mass cut listed above.

After imposing all the cuts, one gets a reduction on the signal event rate which depends on the Higgs mass. For instance, the geometrical acceptance and background rejection cuts (27) account for a reduction factor of 15% for  $m_H = 60$  GeV rising to 25% for  $m_H = 160$  GeV. One must also include in the analysis the particle identification and trigger efficiencies. For leptons and photons they vary from 40% to 70% per particle<sup>39,40</sup>. For the  $jj\gamma\gamma$  final state we estimate the total effect of these efficiencies to be 35%. We therefore obtain an overall efficiency for the  $jj\gamma\gamma$  final state of 5.5% to 9% for  $m_H = 60\text{--}160$  GeV.

Next one must consider the possible backgrounds which contribute to the same final state. The dominant physics background is a mixed QCD-QED process which is automatically included since the calculation is done adding all the SM plus anomalous amplitudes. When the cuts (27) and the efficiencies discussed above are included, this background is reduced to less than 0.2 events for the present luminosity. Dominant backgrounds, however, are due to misidentification when a jet fakes a pho-

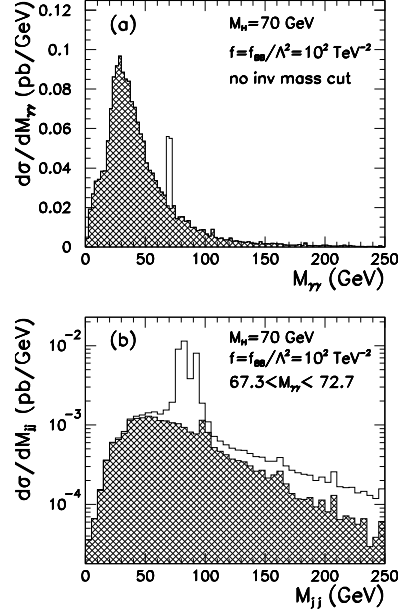


Fig. 8. (a) Two photon invariant mass distribution for the background (shaded histogram) and for the signal (clear histogram) before applying any cut, for  $m_H = 70$  GeV and  $f_{BB}/\Lambda^2 = 100 \text{ TeV}^{-2}$ . (b) Two jet invariant mass distribution, after the cut on the two photon invariant mass.

ton. The probability for a jet to fake a photon has been estimated to be of a few times  $10^{-4}$  <sup>39</sup>. Although this probability is small, it becomes the main source of background for the  $jj\gamma\gamma$  final state because of the very large multijet cross section. In Ref. <sup>31</sup> this background is estimated to lead to  $3.5 \pm 1.3$  events with invariant mass  $M_{\gamma\gamma} > 60$  GeV and it has been consistently included in the derivation of the attainable limits presented below.

The results of this analysis can be used to place limits on the coefficients of the higher-dimension operators. Since DØ report that no event with two-photon invariant mass in the range  $60 < M_{\gamma\gamma} < 220$  has been observed, a 95% CL in the determination of the anomalous coefficient  $f_i$ ,  $i = WW, BB, W, B$  is attained requiring 3 events coming only from the anomalous contributions.

In Fig. 9.a we present the region in the  $f_{WW}, f_{BB}$  plane that can be excluded at 95 % CL in scenario (i), this is, assuming that these are the only non-vanishing couplings, for  $m_H = 100$  GeV. Since the anomalous contribution to  $H\gamma\gamma$  is zero for  $f_{BB} = -f_{WW}$ , the bounds become very weak close to this axis, as clearly shown in Fig. 9. We should remind that these couplings cannot be restricted by the direct searches of gauge-boson production discussed in Sec. 2.3

In order to reduce the number of free parameters one can make the assumption that all blind operators affecting the Higgs interactions have a common coupling  $f$ , *i.e.*  $f = f_W = f_B = f_{WW} = f_{BB}$  (scenario (ii)). We present in Table 1 the 95% CL allowed values of the anomalous couplings in this scenario for different Higgs

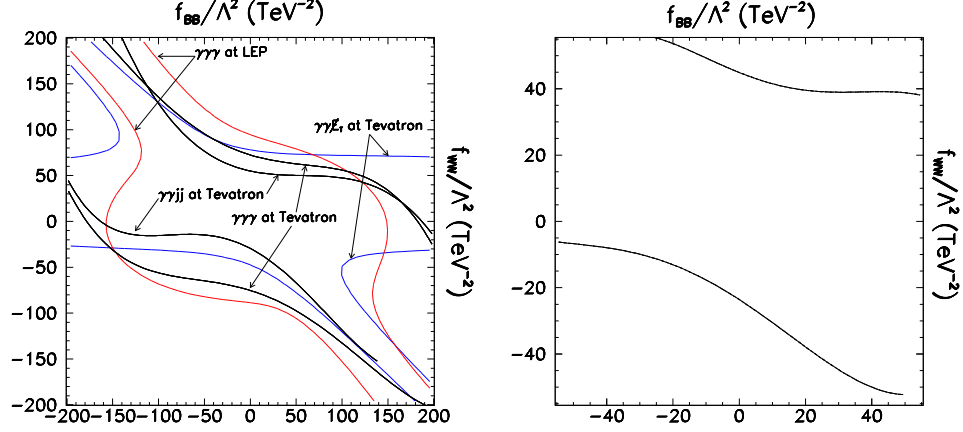


Fig. 9. (a) Exclusion region outside the curves in the  $f_{BB} \times f_{WW}$  plane, in  $\text{TeV}^{-2}$ , based on the DØ analysis<sup>31</sup> of  $\gamma\gamma jj$  production, on the DØ analysis<sup>32</sup> of  $\gamma\gamma \cancel{E}_T$ , on the CDF analysis<sup>33</sup> of  $\gamma\gamma\gamma$  production, and on the OPAL analysis<sup>30</sup> of  $\gamma\gamma\gamma$  production, always assuming  $m_H = 100$  GeV. The curves show the 95% CL deviations from the SM total cross section. (b) Same as (a) for the combined analysis. Notice the change of scale in the last plot.

boson masses. In this scenario these limits lead to constraints on the triple gauge-boson coupling parameters and can be compared with the constraints presented in Eq. (16). We will go back to this comparison when presenting the combined results from the different processes discussed in this section. As expected the limits become

Table 1. 95% CL allowed range for  $f/\Lambda^2$ , from  $\gamma\gamma\gamma$  production at LEP OPAL data and Tevatron CDF data analysis, from  $\gamma\gamma + \cancel{E}_T$  Tevatron DØ data analysis, and from  $\gamma\gamma jj$  Tevatron DØ data analysis in scenario (ii). We denote by — limits worse than  $|f| = 200 \text{ TeV}^{-2}$ .

$m_H(\text{GeV})$	$f/\Lambda^2(\text{TeV}^{-2})$			
	$e^+e^- \rightarrow \gamma\gamma\gamma$	$p\bar{p} \rightarrow \gamma\gamma\gamma$	$p\bar{p} \rightarrow \gamma\gamma + \cancel{E}_T$	$p\bar{p} \rightarrow \gamma\gamma jj$
100	(-64, 57)	(-62, 65)	(-28, 57)	(-16, 42)
120	(-82, 70)	(-76, 77)	(-37, 62)	(-19, 46)
140	(-192, 175)	(-92, 93)	(-48, 72)	(-26, 49)
160	(—, —)	(-113, 115)	(-62, 84)	(-33, 56)
180	(—, —)	(—, —)	(-103, 123)	(-63, 81)
200	(—, —)	(—, —)	(-160, 164)	(-96, 99)
220	(—, —)	(—, —)	(—, —)	(-126, 120)

weaker as the Higgs becomes heavier due to the decrease of the Higgs production cross section.

#### 4.3. $p\bar{p} \rightarrow \gamma\gamma \cancel{E}_T$

We examine next the process  $p\bar{p} \rightarrow \gamma\gamma \cancel{E}_T$ . The dominant anomalous contribution to this final state when the two photons have large invariant mass arises from Higgs- $W(Z)$  associated production<sup>13</sup> as displayed in Fig. 10 where the lepton  $[\ell] = e, \mu$  from  $W$  decay escapes undetected.

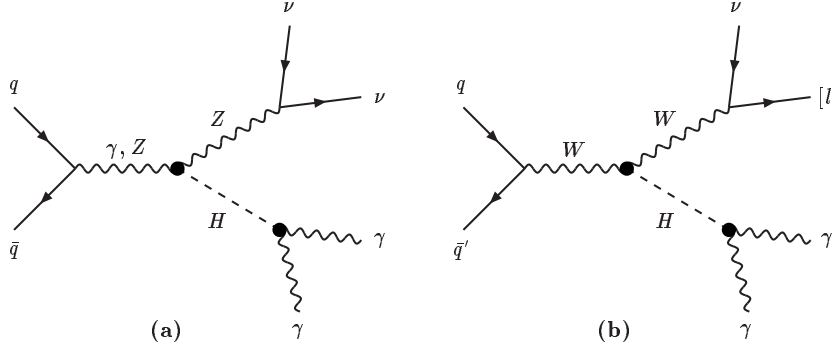


Fig. 10. Dominant anomalous contribution for  $p\bar{p} \rightarrow \gamma\gamma \cancel{E}_T$  production.

The DØ collaboration have searched for diphoton events with large missing transverse energy in  $p\bar{p}$  collisions at  $\sqrt{s} = 1.8$  TeV<sup>32</sup>. Their analysis indicates a good agreement with the expectations from the Standard Model (SM). In this way, the DØ Collaboration were able to set limits on the new physics contribution to the cross section  $\sigma(p\bar{p} \rightarrow \gamma\gamma \cancel{E}_T + X)$ .

In order to compare the theoretical predictions in the presence of the higher-dimension operators with the data collected by the DØ experiment, we must apply the same cuts of Ref.<sup>32</sup>. They require that one photon has transverse energy  $E_T^{\gamma_1} > 20$  GeV and the other  $E_T^{\gamma_2} > 12$  GeV, each of them with pseudorapidity in the range  $|\eta^\gamma| < 1.2$  or  $1.5 < |\eta^\gamma| < 2.0$ . They further require that  $\cancel{E}_T > 25$  GeV. For the  $\ell\nu\gamma\gamma$  final state, one must impose that the charged lepton is outside the covered region of the electromagnetic calorimeter and it escapes undetected ( $|\eta_e| > 2$  or  $1.1 < |\eta_e| < 1.5$ ,  $|\eta_\mu| > 1$ ). After these cuts we find that 80% to 90% of the signal comes from associated Higgs–Z production while 10% to 20% arises from Higgs–W. One must also include in the calculation the particle identification and trigger efficiencies which vary from 40% to 70% per photon<sup>40</sup>. We estimate the total effect of these efficiencies to be 35%<sup>13</sup>.

Next one must consider the possible backgrounds which contribute to the same final state. The main sources of background to this reaction<sup>32</sup> arise from SM processes containing multijets, direct photon,  $W + \gamma$ ,  $W + j$ ,  $Z \rightarrow ee$  and  $Z \rightarrow \tau\tau \rightarrow ee$  where photons are misidentified and/or the missing energy is mismeasured. The DØ collaboration estimate the contribution of all these backgrounds to yield  $2.3 \pm 0.9$  events. DØ have observed two events that have passed the above cuts in their data sample of  $106.3 \pm 5.6$  pb<sup>-1</sup>. The invariant mass of the photon pair in these events are 50.4, and 264.3 GeV.

The results of this analysis can be used to place limits on the coefficients of the higher-dimension operators. Since DØ report that no event with two-photon invariant mass in the range  $60 < M_{\gamma\gamma} < 260$  was observed, a 95% CL in the

determination of the anomalous coefficient  $f_i$ ,  $i = WW, BB, W, B$  is obtained by requiring 3 events coming only from the anomalous contributions.

In Fig. 11, we present the exclusion region in the  $f_{WW} \times f_{BB}$  plane, when we assume that just these two coefficients are different from zero (scenario (i)). The clear (dark) shadow represents the excluded region, at 95% CL, for  $m_H = 80$  (140) GeV. In Table 1 we give the 95% CL allowed values of the anomalous couplings in

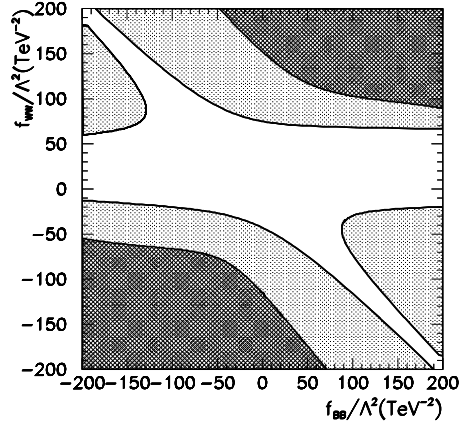


Fig. 11. Excluded region at 95% of CL in the  $f_{WW} \times f_{BB}$  plane, for an integrated luminosity of  $100 \text{ pb}^{-1}$ , and for  $m_H = 80(140) \text{ GeV}$  [light shadow (dark shadow)].

scenario (ii) *i.e.*  $f = f_W = f_B = f_{WW} = f_{BB}$  for different Higgs boson masses. The limits derived from this process are weaker than those from  $p\bar{p} \rightarrow jj\gamma\gamma$  due to the larger decay rate of  $Z$  and  $W$  into jets.

#### 4.4. $p\bar{p} \rightarrow \gamma\gamma\gamma$

We concentrate now in the process  $p\bar{p} \rightarrow \gamma\gamma\gamma$ . The dominant anomalous contribution to this final state for hard photons come from production of a Higgs boson in association with a photon and the subsequent decay of the Higgs into photons <sup>14</sup> displayed in Fig. 12.

The CDF Collaboration <sup>33</sup> have searched for  $\gamma\gamma\gamma$  events with two photons in the central region of the detector ( $|\eta| < 1$ ), with a minimum transverse energy of 12 GeV, plus an additional photon with  $E_T > 25 \text{ GeV}$ . The photons were required to be separated by an angle larger than  $15^\circ$ . After applying these cuts, no event was observed, while the expected number from the background is  $0.1 \pm 0.1$  in the  $85 \text{ pb}^{-1}$  collected. Therefore, at 95 % CL this experimental result implies that the signal should have less than 3 events. The efficiency of identification of an isolated photon is  $68 \pm 3\%$ , for  $E_T > 12 \text{ GeV}$ , and grows to  $84 \pm 4\%$ , for  $E_T > 22 \text{ GeV}$ . When computing the contribution from the higher-dimension operators to this process we

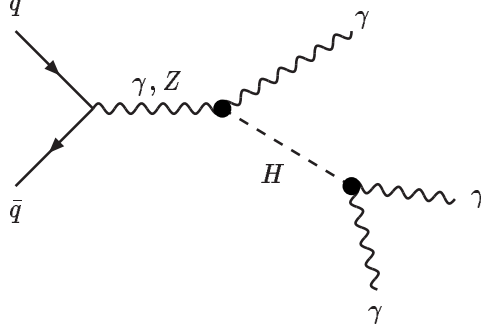


Fig. 12. Dominant anomalous contribution for  $p\bar{p} \rightarrow \gamma\gamma\gamma$  production.

must include the same cuts and efficiencies.

It is important to notice that the dimension–six operators listed in Sec. 2 do not induce 4–point anomalous couplings like  $ZZ\gamma\gamma$ ,  $Z\gamma\gamma\gamma$ , and  $\gamma\gamma\gamma\gamma$ , being these terms generated only by dimension–eight and higher operators. Since the process  $p\bar{p} \rightarrow \gamma\gamma\gamma$  involves the product of two dimension–six operators, we should, in principle, include also in our calculations dimension–eight operators that contribute to the above processes at the same order in the effective Lagrangian expansion. Notwithstanding, we can neglect the higher–order interactions and bound the dimension–six couplings under the naturalness assumption that no cancelation takes place amongst the dimension–six and –eight contributions that appear at the same order in the expansion.

We can now proceed and examine which are the bounds that can be placed on the anomalous coefficients from the negative search of 3 photon events made by the CDF experiment. We start by assuming that the only non–zero coefficients are the ones that generate the anomalous  $H\gamma\gamma$ , *i.e.*,  $f_{BB}$  and  $f_{WW}$  (scenario (i)). The results for the 95% CL exclusion region in the plane  $f_{BB} \times f_{WW}$ , obtained from the CDF data, are presented in Fig. 9.

Finally in Table 1 we give the 95% CL allowed values of the anomalous couplings in scenario (ii) *i.e.*  $f = f_W = f_B = f_{WW} = f_{BB}$  for different Higgs boson masses. As expected the bounds derived from this process are weaker than the ones discussed in Sec. 4.2 and 4.3. This is due to the fact that the anomalous Higgs contribution to the  $\gamma\gamma\gamma$  final state involves the product of two dimension–six operators and it is therefore suppressed by  $1/\Lambda^4$ .

#### 4.5. $e^+e^- \rightarrow \gamma\gamma\gamma$ and $e^+e^- \rightarrow \gamma\gamma + \text{hadrons}$

The effect of the dimension-six operators in Higgs signatures can also be studied at  $e^+e^-$  collisions at LEP II. Due to the lower center-of-mass energy, the dominant contribution for Higgs production is expected from associated production of Higgs with low mass particles. We concentrate here on the processes:

$$e^+e^- \rightarrow \gamma\gamma\gamma, \quad (28)$$

$$e^+e^- \rightarrow \gamma\gamma + \text{hadrons}. \quad (29)$$

The Feynman diagrams describing the anomalous contributions to the above reactions are displayed in Fig. 13. The OPAL collaboration searched for these final

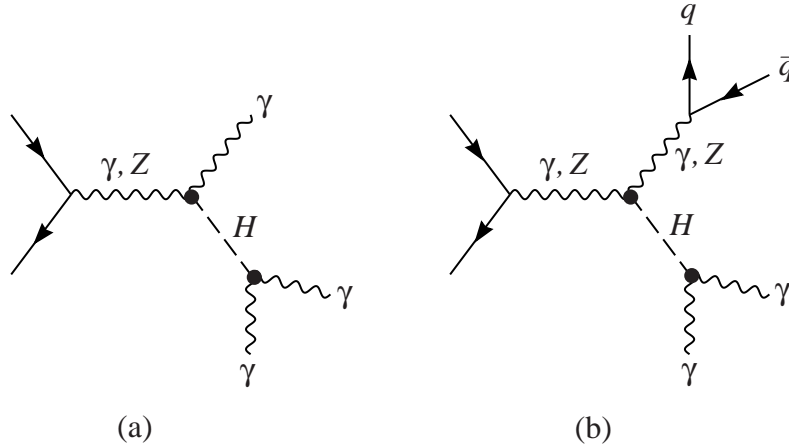


Fig. 13. Anomalous contribution for (a)  $\gamma\gamma\gamma$  production and (b)  $\gamma\gamma$  in association with hadrons.

states. In Refs. <sup>41,30</sup>, data taken at several energy points in the range  $\sqrt{s} = 130$  (91)–172, for the  $\gamma\gamma\gamma$  ( $\gamma\gamma + \text{hadrons}$ ) are combined in order to impose a limit on the cross section for this process as a function of the  $\gamma\gamma$  invariant mass. In order to use OPAL results we must also combine the expected number of events in the presence of the anomalous operators for the corresponding energies and accumulated luminosities.

As for the process  $p\bar{p} \rightarrow \gamma\gamma\gamma$ , in  $e^+e^- \rightarrow \gamma\gamma\gamma$  the production and decay of the Higgs boson also involve two dimension-six operators and we should, in principle, include in our calculations dimension-eight operators that contribute to the above processes. As before we neglect the higher order interactions and bound the dimension-six couplings under the naturalness assumption that no cancellation takes place amongst the dimension-six and -eight contributions that appear at the same order in the expansion.

Assuming that the only non-zero coefficients are the ones that generate the anomalous  $H\gamma\gamma$ , *i.e.*,  $f_{BB}$  and  $f_{WW}$  (scenario (i)). we obtain the excluded region showed in Fig. 14. For small Higgs masses (see Fig. 14) the  $Z$ , which decays hadronically, can be produced on mass shell and, therefore, the strongest bounds come



from the diphoton production in association with hadrons. For higher Higgs-boson masses ( $m_H > 80$  GeV), the  $Z$  cannot be on-mass shell, and the  $\gamma\gamma$  production accompanied by hadrons is suppressed. In this case, only the  $\gamma\gamma\gamma$  final state is able to lead to new bounds. Moreover, the anomalous production of a  $H\gamma$  pair is also suppressed by the phase space as  $m_H$  increases and the limits worsen. It is interesting to notice that the bounds obtained using the above processes are of the same order of the ones that can be extracted from the Tevatron collider for small Higgs boson masses ( $m_H < 80$  GeV).

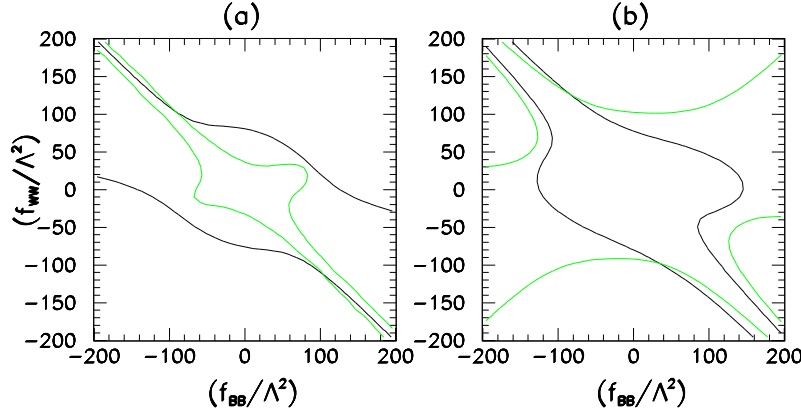


Fig. 14. Contour plot of  $f_{BB} \times f_{WW}$ , in  $\text{TeV}^{-2}$ . The curves show the 95% CL deviations from the SM total cross section, for  $e^+e^- \rightarrow \gamma\gamma\gamma$  (dark lines) and  $e^+e^- \rightarrow q\bar{q}\gamma\gamma$  (light lines) for (a)  $m_H = 60$  GeV and (b)  $m_H = 80$  GeV. The excluded regions are outside the lines

We present in Table 2 the 95% CL allowed regions of the anomalous couplings in scenario (ii). In this framework, the bounds become weaker with the increase of

Table 2. Allowed range of  $f/\Lambda^2$  in  $\text{TeV}^{-2}$  at 95% CL coming from the processes  $e^+e^- \rightarrow \gamma\gamma\gamma$  and  $e^+e^- \rightarrow q\bar{q}\gamma\gamma$  at LEP II. We assumed the scenario defined by Eq. (7).

$m_H(\text{GeV})$	$e^+e^- \rightarrow \gamma\gamma\gamma$	$e^+e^- \rightarrow q\bar{q}\gamma\gamma$
60	( -56 , 50 )	( -24 , 35 )
80	( -53 , 49 )	( -107 , 128 )
100	( -64 , 57 )	( -730 , 750 )
120	( -82 , 70 )	—
140	( -192 , 175 )	—

the Higgs boson mass. The production of diphotons in association with hadrons is again important only when it is possible to produce a pair  $HZ$  on mass shell.

#### 4.6. Combined results: discussion

So far we have presented the limits on anomalous dimension-six Higgs boson in-

teractions that can be derived from the study of several signatures at LEP II and Tevatron colliders. These results obtained from the analysis of the four reactions (25) can be statistically combined in order to obtain a better bound on the coefficient of the effective operators (7) <sup>43</sup>. We exhibit in Fig. 9.b the 95% CL exclusion region in the plane  $f_{BB} \times f_{WW}$  obtained from combined results in scenario (i) for  $m_H = 100$  GeV. In Fig. 15, we present the combined limits for the coupling constant  $f = f_{BB} = f_{WW} = f_B = f_W =$  (scenario (ii)) for Higgs boson masses in the range of  $100 \leq m_H \leq 220$  GeV. In this scenario  $\alpha_{W\phi} = \alpha_{B\phi} = \alpha = \frac{m_W^2}{2\Lambda^2} f$ .

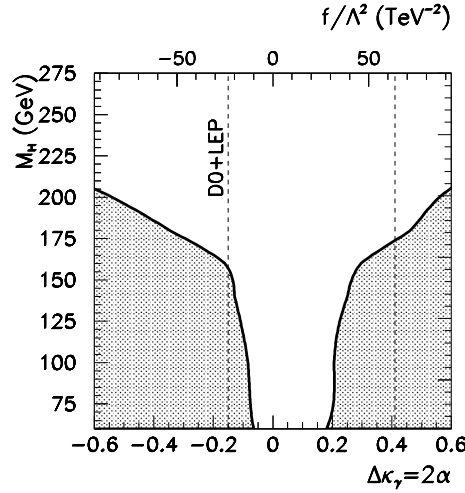


Fig. 15. Excluded region in the  $f \times m_H$  plane from the combined analysis from the combined results of the  $\gamma\gamma\gamma$  production at LEP II,  $\gamma\gamma\gamma$ ,  $\gamma\gamma + \cancel{e}^+e^-$ , and  $\gamma\gamma jj$  production at Tevatron, assuming that all  $f_i$  are equal (see text for details).

We can compare now these results with the existing limits on the coefficients of dimension-six operators (see Sec. 2.3) As discussed in Sec. 2.1 for linearly realized effective Lagrangians, the modifications introduced in the Higgs and in the vector boson sector are related to each other. In consequence the bounds on the new Higgs couplings should also restrict the anomalous gauge-boson self-interactions. Under the assumption of equal coefficients for all anomalous Higgs operators, we can relate the common Higgs boson anomalous coupling  $f$  with the conventional parametrization of the vertex  $WWV$  ( $V = Z^0, \gamma$ ),

$$\begin{aligned} \Delta\kappa_\gamma &= \frac{m_W^2}{\Lambda^2} f, \\ \Delta\kappa_Z &= \frac{m_Z^2}{2\Lambda^2} (1 - 2s_W^2) f, \\ \Delta g_1^Z &= \frac{m_Z^2}{2\Lambda^2} f. \end{aligned} \tag{30}$$

In Table 3, we present the 95% CL limit of the anomalous coupling  $\Delta\kappa_\gamma$  using the

limits on  $f/\Lambda^2$  obtained through the analysis of the processes considered above. We also present the expected bounds that will be reachable at the upgraded Tevatron and at the NLC which will be discussed next. These results show that the present combined limit from the Higgs production analysis is comparable with the existing bound from gauge–boson production (16) for  $m_H \leq 170$  GeV.

Table 3. 95% CL allowed range for the anomalous triple gauge–boson couplings derived from the limits obtained for the anomalous Higgs boson coupling  $f$ .

Process	$m_H$ (GeV)	$\Delta\kappa_\gamma = 2\alpha = 2\alpha_{B\Phi} = 2, \alpha_{W\Phi}$
Combined Tevatron RunI + LEP II	100	(−0.084 , 0.204 )
Combined Tevatron RunII	100	(−0.048 , 0.0122 )
Combined Tevatron TeV33	100	(−0.020 , 0.036 )
$e^+e^- \rightarrow W^+W^-\gamma$ at NLC	200	(−0.020 , 0.026 )
$e^+e^- \rightarrow Z^0Z^0\gamma$ at NLC	200	(−0.016 , 0.024 )

#### 4.7. Future perspectives

The effect of the anomalous operators becomes more evident with the increase of energy, and higher sensitive to smaller values of the anomalous coefficients can be achieved by studying their contribution to different processes at the upgraded Tevatron collider or at new machines, like the Next Linear Collider.

The analysis of the reactions  $p\bar{p} \rightarrow \gamma\gamma \cancel{E}_T$  and  $p\bar{p} \rightarrow \gamma\gamma jj$  presented before can be repeated for the upgraded Tevatron collider. We consider here that the upgraded Tevatron Run II will collect an integrated luminosity of  $1 \text{ fb}^{-1}$ , and TeV33 will deliver  $10 \text{ fb}^{-1}$ <sup>42</sup>. In the results presented next we will assume the same cuts and detection efficiencies as given in the previous sections.

For the  $\gamma\gamma\gamma$  final state it is possible to improve the sensitivity to the anomalous coefficients by implementing additional kinematical cuts<sup>14</sup>. Best results are obtained for the following set of cuts:  $E_{T_1} > 40$  GeV, with  $E_{T_{2,3}} > 12$  GeV where the three photons have been ordered according to their transverse energy, *i.e.*  $E_{T_1} > E_{T_2} > E_{T_3}$ . The photons are always required to be in the central region of the detector ( $|\eta_i| < 1$ ) where there is sensitivity for electromagnetic showering. In the estimates presented here the same detection efficiency for photons as considered by the CDF Collaboration is assumed<sup>33</sup>.

Table 4 contains the 95% CL limits on the anomalous couplings that could be achievable at Tevatron Run II and at TeV33 for each individual process. All couplings are assumed equal (scenario *(ii)*) and the Higgs boson mass is varied in the range  $100 \leq m_H \leq 220$  GeV. The combination of the results obtained from the analysis of the three reactions leads to the improved bounds given in Table 5. Comparing these results with those in Fig. 15 we observe an expected improvement of about a factor  $\sim 2$ – $3$  [ $\sim 4$ – $6$ ] for the combined limits at RunII [TeV33].

The Next Linear electron–positron Collider will open an important opportunity to further improve the search for new physics. In particular, the anomalous Higgs

Table 4. 95% CL allowed range for  $f/\Lambda^2$ , from  $\gamma\gamma\gamma$ ,  $\gamma\gamma + \cancel{E}_T$ ,  $\gamma\gamma jj$  production at Tevatron Run II [TeV33] assuming all  $f_i$  to be equal. We denote by — limits worse than  $|f| = 100 \text{ TeV}^{-2}$ .

$m_H(\text{GeV})$	$f/\Lambda^2(\text{TeV}^{-2})$		
	$p\bar{p} \rightarrow \gamma\gamma\gamma$	$p\bar{p} \rightarrow \gamma\gamma + \cancel{E}_T$	$p\bar{p} \rightarrow \gamma\gamma jj$
100	( -24 , 24 ) [ -13 , 15 ]	( -16 , 36 ) [ -9.4 , 26 ]	( -9.2 , 22 ) [ -3.3 , 5.6 ]
120	( -26 , 26 ) [ -14 , 14 ]	( -20 , 39 ) [ -15 , 27 ]	( -8.6 , 21 ) [ -3.4 , 5.9 ]
140	( -30 , 31 ) [ -15 , 16 ]	( -25 , 44 ) [ -14 , 30 ]	( -10 , 23 ) [ -4.5 , 8.9 ]
160	( -36 , 38 ) [ -17 , 19 ]	( -29 , 50 ) [ -14 , 33 ]	( -11 , 24 ) [ -6.0 , 14 ]
180	( — , — ) [ — , — ]	( -63 , 72 ) [ -46 , 53 ]	( -26 , 34 ) [ -16 , 24 ]
200	( — , — ) [ — , — ]	( -87 , 90 ) [ -50 , 53 ]	( -33 , 40 ) [ -17 , 23 ]
220	( — , — ) [ — , — ]	( — , — ) [ — , — ]	( -42 , 45 ) [ -19 , 26 ]

Table 5. 95% CL allowed range for  $f/\Lambda^2$ , from the combinations of  $\gamma\gamma\gamma$ ,  $\gamma\gamma + \cancel{E}_T$ ,  $\gamma\gamma jj$  production at Tevatron Run II [TeV33] assuming all  $f_i$  to be equal.

$m_H(\text{GeV})$	$f/\Lambda^2(\text{TeV}^{-2})$	
	COMBINED	
100	( -7.6 , 19 ) [ -3 , 5.6 ]	
120	( -7.4 , 18 ) [ -3.3 , 5.9 ]	
140	( -9.1 , 20 ) [ -4.0 , 8.7 ]	
160	( -9.9 , 22 ) [ -5.1 , 13 ]	
180	( -24 , 33 ) [ -16 , 24 ]	
200	( -32 , 39 ) [ -17 , 23 ]	
220	( -42 , 45 ) [ -19 , 26 ]	

boson couplings can be investigated in the processes <sup>10,11</sup>:

$$e^+e^- \rightarrow W^+W^-\gamma, \quad (31)$$

$$e^+e^- \rightarrow Z^0Z^0\gamma. \quad (32)$$

We discuss here the sensitivity of NLC to these processes assuming a center-of-mass energy of  $\sqrt{s} = 500 \text{ GeV}$  and an integrated luminosity  $\mathcal{L} = 50 \text{ fb}^{-1}$ . In order to account for standard detector effects a cut in the photon energy of  $E_\gamma > 20 \text{ GeV}$  was adopted and the angle between any two particles was required to be larger than  $15^\circ$ .

One can investigate the different distributions of the final state particles in order to search for kinematical cuts that could improve the NLC sensitivity. The most promising variable is the photon transverse momentum as the contribution of the anomalous couplings is larger in the high  $p_{T_\gamma}$  region. This is understood because the anomalous signal is dominated by on-mass-shell Higgs- $\gamma$  production with the subsequent  $H \rightarrow W^+W^-$  or  $Z^0Z^0$  decay and the photon transverse momentum is distributed around the monochromatic peak  $E_\gamma^{\text{mono}} = (s - m_H^2)/(2\sqrt{s})$ . In consequence for Higgs boson masses in the range  $2m_{W,Z} \leq m_H \leq (\sqrt{s} - E_\gamma^{\text{min}}) \text{ GeV}$ , where on-shell production is allowed, a cut of  $p_{T_\gamma} > 100$  drastically reduces the background. For lighter Higgs bosons, *e.g.*  $m_H < 2m_{W,Z}$ , the  $p_{T_\gamma}$  cut is ineffective since the Higgs boson is off-mass-shell and the peak in the photon transverse momentum distribution disappears. This makes the attainable bounds on the anoma-

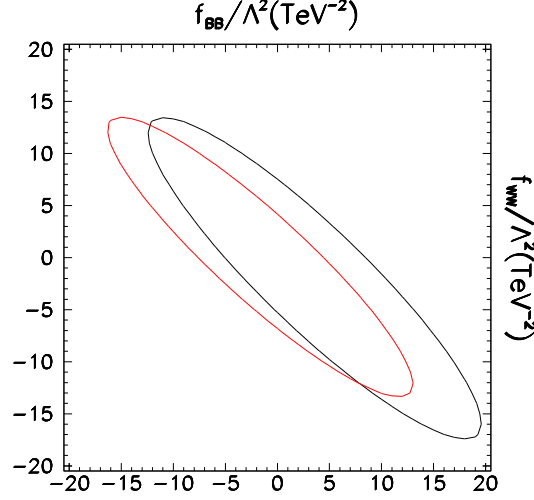


Fig. 16. Contour plot of  $f_{BB} \times f_{WW}$ , from  $e^+e^- \rightarrow W^+W^-\gamma$  (black line) and  $e^+e^- \rightarrow Z^0Z^0\gamma$  (red line) at NLC, for  $m_H = 200$  GeV with a cut of  $p_{T\gamma} > 100$  GeV. The curves show the 95% CL deviations from the SM total cross section.

Table 6. 95% CL allowed range for  $f/\Lambda^2$ , from  $W^+W^-\gamma$  and  $Z^0Z^0\gamma$  production at NLC, assuming all  $f_i$  to be equal.

$m_H(\text{GeV})$	$f/\Lambda^2(\text{TeV}^{-2})$	
	$e^+e^- \rightarrow W^+W^-\gamma$ at NLC	$e^+e^- \rightarrow Z^0Z^0\gamma$ at NLC
170	(-2.3 , 3.7)	( — , — )
200	(-3.2 , 4.0)	(-2.6 , 3.9)
250	(-4.3 , 4.8)	(-3.2 , 4.3)
300	(-6.3 , 6.3)	(-4.7 , 5.2)
350	(-12 , 9.5)	(-7.1 , 8.3)

lous coefficients that could be obtained from the  $W^+W^-(Z^0Z^0)\gamma$  production to be very loose.

In Fig. 16 we show the region in the plane  $f_{BB} \times f_{WW}$  for  $m_H = 200$  GeV that could be excluded at 95% CL from the study of reactions (31) and (32). Notice that for these two reactions the exclusion region closes the gap at  $f_{BB} = -f_{WW}$  since the anomalous decay widths  $H \rightarrow W^+W^-(Z^0Z^0)$  do not vanish along this axis as we have seen in Sec. 3.2.

We present in Table 6 the sensitivity to the coefficient  $f/\Lambda^2$  based on a 95% CL deviation in the total cross section for a Higgs mass in the range  $170 \leq m_H \leq 350$  GeV in scenario (ii). The results coming from the  $Z^0Z^0\gamma$  production are a little better than the ones obtained from  $W^+W^-\gamma$  production, and they can improve by one order of magnitude the actual limits derived from LEP and Tevatron data analyses.

## 5. Conclusions

A consistent description of the effect of new physics in the bosonic sector of the SM

in terms of effective Lagrangians, implies the presence of anomalous Higgs couplings to the gauge bosons. In this review we have concentrated on the effects of these new interactions on the Higgs boson phenomenology.

In the effective Lagrangian language, we have described the effects of the new physics at low energy by including in the Lagrangian higher-dimension operators. In building these operators we have used a linear realization of the  $SU(2)_L \times U(1)_Y$  gauge symmetry and we have included all operators  $C$  and  $P$  invariant constructed out of the gauge-boson and the Higgs fields while keeping the fermionic sector unchanged. Such effective Lagrangian contains eleven dimension-six operators with unknown coefficients. Four of these operators,  $\mathcal{O}_{\Phi,1}$ ,  $\mathcal{O}_{DW}$ ,  $\mathcal{O}_{DB}$ , and  $\mathcal{O}_{BW}$ , modify the gauge-boson two-point functions at tree level while three operators,  $\mathcal{O}_{WW}$ ,  $\mathcal{O}_W$ , and  $\mathcal{O}_B$ , enter at lower order in the gauge-boson three-point functions. We have summarized the constraints on these operators arising from their contributions to existing low-energy observables as well as to the direct gauge-boson production at the Tevatron Collider and LEP II.

The operators  $\mathcal{O}_{WW}$ ,  $\mathcal{O}_{BB}$ ,  $\mathcal{O}_W$ , and  $\mathcal{O}_B$ , enter at lower order in the Higgs couplings to the gauge bosons. Most of this review is concentrated on the study of the effects of these operators on the Higgs boson signatures, and on the possibility of constraining their coefficients by using the negative results of searches at LEP II and the Tevatron colliders. One of the most interesting features associated with the presence of these operators is the enhancement of the Higgs decay rate in two photons what makes the Higgs searches particularly clean at hadron colliders. We have shown how the use of the results from searches of final states containing photons such as :  $p\bar{p} \rightarrow jj\gamma\gamma$ ,  $p\bar{p} \rightarrow \gamma\gamma + \cancel{E}_T$ ,  $p\bar{p} \rightarrow \gamma\gamma\gamma$  and  $e^+e^- \rightarrow \gamma\gamma\gamma$  at the Tevatron and LEP II can be used to place limits on the values of the coefficients of the higher-dimension operators, or, in other words, on the scale of new physics. Since we have concentrated on the effects associated with the Higgs decay into photons which involve the operators  $\mathcal{O}_{WW}$  and  $\mathcal{O}_{BB}$ , the bounds apply undoubtedly to the coefficients of those operators. The limits on these coefficients are summarized in Fig. 9.

The operators  $\mathcal{O}_W$ , and  $\mathcal{O}_B$  modify both the Higgs production rates as well as the gauge boson self-couplings. We have discussed how if we further assume that the coefficients of the four operators  $\mathcal{O}_{WW}$  and  $\mathcal{O}_{BB}$ ,  $\mathcal{O}_W$ , and  $\mathcal{O}_B$  are equal, both effects can be compared. The limits obtained from Higgs boson searches under this assumption are summarized in Tables 1, 3, and in Fig. 15. Under the assumption of equal coefficients for all anomalous Higgs operators, we can relate the common Higgs boson anomalous coupling  $f$  with the conventional parametrization of the vertex  $WWV$  with  $\Delta\kappa_\gamma = m_W^2/\Lambda^2 f$ . The present combined limit from the Higgs production analysis is comparable with the existing bound from gauge-boson production for  $m_H \leq 170$  GeV. We have also discussed how the sensitivity to anomalous Higgs couplings can be expected to improve by a factor 2–6 at future Tevatron runs and by about one order of magnitude at the the NLC and it will reach close to the strong bounds on the four “not-blind” operators that contribute

to the four-fermion amplitudes at tree level.

### Acknowledgements

I wish to thank all my collaborators in the subject of anomalous higgs couplings: F. de Campos, O.J.P. Eboli, S. Lietti, S.F. Novaes, and R. Rosenfeld. I also want to thank R. Vazquez for his careful reading of the manuscript and for many useful comments and suggestions. It is also a pleasure to acknowledge the Instituto de Fisica Teorica de la Universidade Estadual Paulista in Sao Paulo, Brazil, for their warm hospitality during my stays there when most of the results included in this review were obtained. This work was supported by grants CICYT AEN96-1718, DGICYT PB95-1077 and DGICYT PB97-1261, by the EEC under the TMR contract ERBFMRX-CT96-0090 and by Fundação de Amparo à Pesquisa do Estado de São Paulo (FAPESP).

### References

- [1] See, for instance: G. Altarelli, preprint CERN-TH.97-278, and e-Print Archive hep-ph/9710434; D. Karlen, plenary talk at the *XXIX International Conference of High Energy Physics*, Vancouver, BC, Canada, July 23–29, 1998.
- [2] S. Weinberg, *Physica* **96A**, 327 (1979); see also H. Georgi, *Weak Interactions and Modern Particle Theory* (Benjamin/Cummings, Menlo Park, 1984) and J. F. Donoghue, E. Golowich and B. R. Holstein, *Dynamics of the Standard Model* (Cambridge University Press, 1992).
- [3] T. Appelquist and C. Bernard, *Phys. Rev.* **D22**, 200 (1980); A. Longhitano, *Phys. Rev.* **D22**, 1166 (1980); *Nucl. Phys.* **B188**, 118 (1981).
- [4] W. Buchmüller and D. Wyler, *Nucl. Phys.* **B268**, 621 (1986); C. J. C. Burgess and H. J. Schnitzer, *Nucl. Phys.* **B228**, 454 (1983); C. N. Leung, S. T. Love and S. Rao, *Z. Phys.* **31**, 433 (1986); A. De Rújula, M. B. Gavela, P. Hernández and E. Massó, *Nucl. Phys.* **B384**, 3 (1992).
- [5] K. Hagiwara, S. Ishihara, R. Szalapski and D. Zeppenfeld, *Phys. Lett.* **B283**, 353 (1992); *idem*, *Phys. Rev.* **D48**, 2182 (1993).
- [6] K. Hagiwara, R. Szalapski and D. Zeppenfeld, *Phys. Lett.* **B318**, 155 (1993).
- [7] K. Hagiwara and M. L. Stong, *Z. Phys.* **62**, 99 (1994); B. Grzadowski and J. Wudka, *Phys. Lett.* **B364**, 49 (1995); G. J. Gounaris, F. M. Renard and N. D. Vlachos, *Nucl. Phys.* **B459**, 51 (1996); W. Killian, M. Krämer and P. M. Zerwas, *Phys. Lett.* **B381**, 243 (1996).
- [8] S. M. Lietti, S. F. Novaes and R. Rosenfeld, *Phys. Rev.* **D54**, 3266 (1996); F. de Campos, S. M. Lietti, S. F. Novaes and R. Rosenfeld, *Phys. Lett.* **B389**, 93 (1996), and Erratum, *Phys. Lett.* **B425**, 413 (1998).
- [9] O. J. P. Éboli, M. C. Gonzalez-Garcia, S. M. Lietti, and S. F. Novaes, *Phys. Lett.* **B434**, 340 (1998).
- [10] F. de Campos, S. M. Lietti, S. F. Novaes, and R. Rosenfeld, *Phys. Rev.* **D56**, 4384 (1997).
- [11] S. M. Lietti and S. F. Novaes, *Phys. Lett.* **B416**, 441 (1998).
- [12] F. de Campos, M. C. Gonzalez-Garcia and S. F. Novaes, *Phys. Rev. Lett.* **79**, 5213 (1997).
- [13] M. C. Gonzalez-Garcia, S. M. Lietti, and S. F. Novaes, *Phys. Rev.* **D57**, 7045 (1998).

- [14] F. de Campos, M. C. Gonzalez-Garcia, S. M. Lietti, S. F. Novaes, and R. Rosenfeld, Phys. Lett. **B435**, 407 (1998).
- [15] G. J. Gounaris, J. Layssac and F. M. Renard, Z. Phys. **69**, 505 (1996); G. J. Gounaris and F. M. Renard, Z. Phys. **69**, 513 (1996).
- [16] P. Hernández and J. Vegas Phys. Lett. **B307**, 116 (1993).
- [17] K. Hagiwara, S. Matsumoto R. Szalapski, Phys. Lett. **B357**, 411 (1995); S. Alam, S. Dawson, R. Szalapski, Phys. Rev. **D57**, 1577 (1998).
- [18] O. J. P. Éboli, S. M. Lietti, M. C. Gonzalez-Garcia, S. F. Novaes, Phys. Lett. **B339**, 119 (1994); For an update see O. J. P. Éboli, M. C. Gonzalez-Garcia, S. F. Novaes, hep-ph/9811388.
- [19] F. M. Renard and C. Verzegnassi, Phys. Lett. **B345**, 500 (1995); S. Dawson and G. Valencia, Nucl. Phys. **B439**, 3 (1995); F. M. Renard, S. Spagnolo, and C. Verzegnassi, Phys. Lett. **B409**, 398 (1997); S. Alam, S. Dawson, and R. Szalapski, Phys. Rev. **D57**, 1577 (1998).
- [20] M. E. Peskin and T. Takeuchi, Phys. Rev. Lett. **65**, 694 (1990); G. Altarelli, R. Barbieri, and F. Caravaglios, Nucl. Phys. **B405**, 3 (1993).
- [21] B. Abbott *et al.*, DØ Collaboration, Phys. Rev. **D58**, 031102 (1998).
- [22] ALEPH Collaboration, R. Barate *et al.*, Phys. Lett. **B422**, 369 (1998); DELPHI Collaboration, P. Abreu *et al.*, Phys. Lett. **B423**, 194 (1998); L3 Collaboration, M. Acciari *et al.*, Phys. Lett. **B413**, 176 (1998); OPAL Collaboration, K. Ackerstaff *et al.*, Eur. Phys. J. **C2**, 597 (1998).
- [23] K. Hagiwara, H. Hikasa, R. D. Peccei and D. Zeppenfeld, Nucl. Phys. **B282**, 253 (1987).
- [24] G. Gounaris, J.-L. Kneur, D. Zeppenfeld (conveners), in “Physics at LEP2”, edited by G. Altarelli, T. Sjöstrand and F. Zwirner, CERN 96-01, Vol. 1, p. 525 (1996), and e-Print Archive hep-ph/9601233.
- [25] ALEPH, DELPHI, L3, OPAL, and DØ Collaborations, LEPEWWG/TGC/98-01 and DØ Note 3437, May 1998; H. T. Diehl, talk given at *XXIX International Conference of High Energy Physics*, Vancouver, BC, Canada, July 23–29, 1998, Fermilab-Pub-98/303-E and e-Print Archive hep-ex/9810006.
- [26] J. Ellis, M. K. Gaillard, D. V. Nanopoulos, Nucl. Phys. **B106**, 292 (1976); M. A. Shifman, A. I. Vainshtein, M. B. Voloshin, V. I. Zakharov, Sov. J. Nucl. Phys. **30**, 711 (1979).
- [27] J. F. Gunion, H. E. Haber, G. Kane, S. Dawson, *The Higgs Hunter’s Guide* (Addison-Wesley, 1990).
- [28] A. Stange, W. Marciano, and S. Willenbrock, Phys. Rev. **D49**, 1354 (1994); Phys. Rev. **D50**, 4491 (1994).
- [29] X. Tata, in the *Proceedings of the IX Jorge André Swieca Summer School: Particles and Fields*, São Paulo, Brazil, edited by J. C. A. Barata, A. Malbouisson, and S. F. Novaes, (World Scientific, Singapore, 1998).
- [30] OPAL Collaboration, K. Ackerstaff *et al.*, Eur. Phys. J. **C1**, 21 (1998).
- [31] B. Abbott *et al.*, DØ Collaboration, talk given at *18th International Symposium on Lepton-Photon Interactions*, Hamburg, Germany (1997), report FERMILAB-CONF-97/325-E.
- [32] S. Abachi *et al.*, DØ Collaboration, Phys. Rev. Lett. **78**, 2070 (1997); B. Abbott *et al.*, DØ Collaboration, Phys. Rev. Lett. **80**, 442 (1998); See also the DØ Collaboration public Web page:  
<http://www-d0.fnal.gov/public/new/analyses/gauge/welcome.html>.
- [33] F. Abe *et al.*, CDF Collaboration, Phys. Rev. Lett. **81**, 1791 (1998).
- [34] T. Stelzer and W. F. Long, Comput. Phys. Commun. **81**, 357 (1994).
- [35] H. Murayama, I. Watanabe and K. Hagiwara, KEK report 91-11 (unpublished).
- [36] A. D. Martin, W. J. Stirling, R. G. Roberts Phys. Lett. **B354**, 155 (1995).

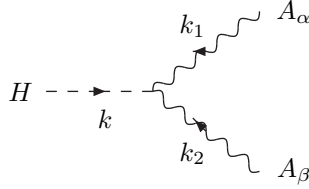


- [37] O. Helene, Nucl. Instr. and Meth. **212**, 319 (1983).
- [38] V. Barger, T. Han, D. Zeppenfeld, and J. Ohnemus, Phys. Rev. **D41**, 2782 (1990).
- [39] S. Abachi *et al.*, DØ Collaboration, Phys. Rev. Lett. **75**, 1023 (1995); *idem* **75**, 1028 (1995); *idem* **75**, 1034 (1995); *idem* **77**, 3303 (1996); *idem* **78**, 3634 (1997); *idem* **78**, 3640 (1997).
- [40] B. Abbott *et al.*, DØ Collaboration, Phys. Rev. Lett. **79**, 1441 (1997).
- [41] OPAL Collaboration, K. Ackerstaff *et al.*, Eur. Phys. J. **C1**, 31 (1998).
- [42] D. Amidei *et al.*, *Future Electroweak Physics at the Fermilab Tevatron: Report of the TeV-2000 Study Group*, preprint FERMILAB-PUB-96-082 (1996).
- [43] M. C. Gonzalez-Garcia, S. M. Lietti, S. F. Novaes, e-Print Archive hep-ph/9811373, to appear in Phys. Rev. D.

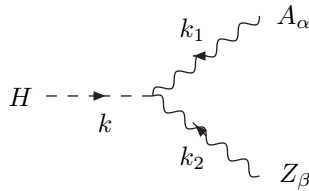
## Appendix A

Here we give the Feynman rules for the triple and quartic vertices from operators listed in Sec. 2.1 We do not include the contributions from “not-blind” operators (4).

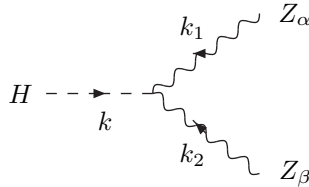
The couplings of the Higgs to gauge bosons are:



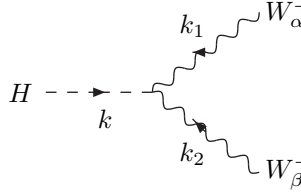
$$i \frac{gm_W}{\Lambda^2} 2s^2 (f_{BB} + f_{WW}) [g^{\alpha\beta} (k_1 \cdot k_2) - k_1^\beta k_2^\alpha]$$



$$i \frac{gm_W}{\Lambda^2} \frac{s}{c} \left\{ 2(s^2 f_{BB} - c^2 f_{WW}) [-g^{\alpha\beta} (k_1 \cdot k_2) + k_2^\alpha k_1^\beta] + \frac{1}{2} (f_W - f_B) [-g^{\alpha\beta} (k_1^2 + k_1 \cdot k_2) + (k_1^\alpha + k_2^\alpha) k_1^\beta] \right\}$$

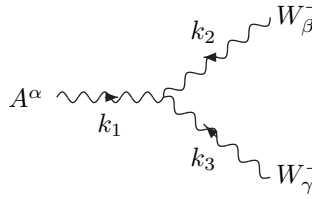


$$i \frac{gm_W}{\Lambda^2} \frac{1}{2c^2} \left\{ 4(s^4 f_{BB} + c^4 f_{WW}) [g^{\alpha\beta} (k_1 \cdot k_2) - k_2^\alpha k_1^\beta] + (c^2 f_W + s^2 f_B) [-g^{\alpha\beta} (k_1^2 + k_2^2 + 2k_1 \cdot k_2) + (k_1^\alpha k_1^\beta + 2k_2^\alpha k_1^\beta + k_2^\alpha k_2^\beta)] \right\}$$

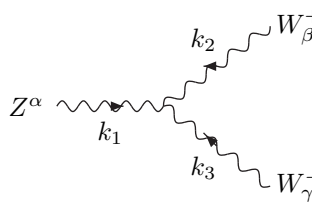


$$i \frac{gm_W}{\Lambda^2} \left\{ \frac{f_W}{2} [(k_1^\alpha k_1^\beta + k_2^\alpha k_2^\beta) - g^{\alpha\beta} (k_1^2 + k_2^2)] + (f_W - 2f_{WW}) [k_2^\alpha k_1^\beta - g^{\alpha\beta} (k_1 \cdot k_2)] \right\}$$

The triple vector boson self-couplings:

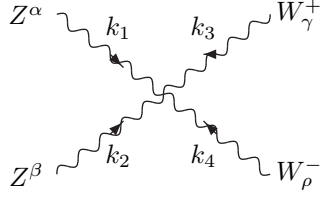


$$i \frac{gs}{2\Lambda^2} \left\{ m_W^2 (f_B + f_W) [g^{\alpha\beta} k_1^\gamma - g^{\alpha\gamma} k_1^\beta] + -3g^2 f_{WWW} \left[ k_1^\beta k_2^\gamma k_3^\alpha - k_1^\gamma k_2^\alpha k_3^\beta + (k_1 \cdot k_2) (g^{\alpha\gamma} k_3^\beta - g^{\beta\gamma} k_3^\alpha) + (k_1 \cdot k_3) (g^{\beta\gamma} k_2^\alpha - g^{\alpha\beta} k_2^\gamma) + (k_2 \cdot k_3) (g^{\alpha\beta} k_1^\gamma - g^{\alpha\gamma} k_1^\beta) \right] \right\}$$

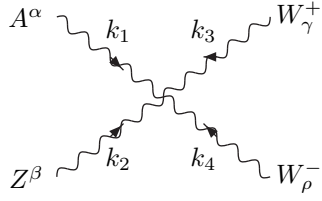


$$i \frac{g}{2\Lambda^2 c} \left\{ -m_W^2 s^2 (f_B + f_W) [g^{\alpha\beta} k_1^\gamma - g^{\alpha\gamma} k_1^\beta] + m_W^2 f_W [g^{\alpha\gamma} (k_3 - k_1)^\beta + g^{\alpha\beta} (k_1 - k_2)^\gamma + g^{\beta\gamma} (k_2 - k_3)^\alpha] + -3g^2 c^2 f_{WWW} \left[ k_1^\beta k_2^\gamma k_3^\alpha - k_1^\gamma k_2^\alpha k_3^\beta + (k_1 \cdot k_2) (g^{\alpha\gamma} k_3^\beta - g^{\beta\gamma} k_3^\alpha) + (k_1 \cdot k_3) (g^{\beta\gamma} k_2^\alpha - g^{\alpha\beta} k_2^\gamma) + (k_2 \cdot k_3) (g^{\alpha\beta} k_1^\gamma - g^{\alpha\gamma} k_1^\beta) \right] \right\}$$

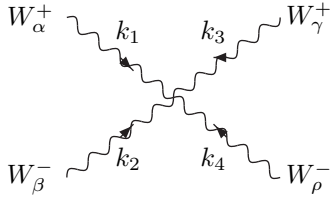
The quartic couplings for the gauge bosons, involve the couplings  $f_W$ ,  $f_{WWW}$  and  $f_{DW}$ . We give here the expressions for  $f_{WWW} = f_{DW} = 0$  which are the relevant ones for our study:



$$i \frac{g^2 m_W^2}{\Lambda^2} f_W \left[ g^{\alpha\gamma} g^{\beta\rho} + g^{\alpha\rho} g^{\beta\gamma} - 2g^{\alpha\beta} g^{\gamma\rho} \right]$$



$$i \frac{g^2 m_W^2 s}{\Lambda^2 c} f_W \left[ g^{\alpha\gamma} g^{\beta\rho} + g^{\alpha\rho} g^{\beta\gamma} - 2g^{\alpha\beta} g^{\gamma\rho} \right]$$



$$-i \frac{g^2 m_W^2}{\Lambda^2} f_W \left[ g^{\alpha\beta} g^{\gamma\rho} + g^{\alpha\rho} g^{\beta\gamma} - 2g^{\alpha\gamma} g^{\beta\rho} \right]$$